geosciences

MDPI

Article

Microstructural Investigation of Variscan Late-Collisional Granitoids (Asinara Island, NW Sardinia, Italy): New Insights on the Relationship Between Regional Deformation and Magma Emplacement

Diego Pieruccioni [1,*], Matteo Simonetti [1], Salvatore Iaccarino [2], Chiara Montomoli [2,3] and Rodolfo Carosi [2]

[1] Geological Survey of Italy, Institute for Environmental Protection and Research (ISPRA), 00144 Roma, Italy; matteo.simonetti@isprambiente.it
[2] Department of Earth Sciences, University of Turin, 10125 Torino, Italy; salvatore.iaccarino@unito.it (S.I.); chiara.montomoli@unito.it (C.M.); rodolfo.carosi@unito.it (R.C.)
[3] CNR-IGG Pisa, Institute of Geosciences and Earth Resources, 56127 Pisa, Italy
* Correspondence: diego.pieruccioni@isprambiente.it

Abstract: In the framework of the geological mapping of sheet "n. 425—Asinara Island" (NW Sardinia, Italy) of the Italian National Geological Mapping Project (CARG Project), three late- to post-collisional Variscan intrusive units are recognized: (i) Castellaccio Unit; (ii) Punta Sabina Unit; and (iii) sheeted dyke complex. Granitoid rocks from these intrusive units intruded into the medium- to high-grade metamorphic micaschist and paragneiss and the migmatitic complex. A range of deformation microstructures from sub-magmatic to low-temperature subsolidus conditions are recognized. The main observed microstructures are represented by chessboard patterns in quartz and by feldspar sub-grain rotation dynamic recrystallization, indicative of deformation at high-temperature conditions (T > 650 °C). Solid-state high-temperature deformations (T > 450 °C) are provided by feldspar bulging, myrmekites, quartz grain boundary migration and sub-grain rotation dynamic recrystallization. Low-temperature sub-solidus microstructures (T < 450 °C) consist of quartz bulging, mica kinks, and feldspar twinning and bending. These features highlight that the three intrusive units recorded tectonic stresses, which affected the granitoids during cooling without developing a strong penetrative meso/microstructural fabric, as observed in other sectors of the Variscan orogen. The complete sequence of deformation microstructures, recorded in all intrusive units, suggests a weak but still ongoing deformation regime during granitoid emplacement in the Variscan orogen of northwestern Sardinia. These observations are similar to the features highlighted in other sectors of the southern Variscan belt and suggest a complex interplay between transpressional-induced exhumation of the middle/deep crust and magma intrusion.

Keywords: deformation microstructures; late-Variscan magmatism; CARG Project; ductile deformation of granitoids; structural analysis; Sardinia

Academic Editors: Salvatore Critelli and Tadeusz Marek Peryt

Received: 24 January 2025
Revised: 24 February 2025
Accepted: 11 March 2025
Published: 18 March 2025

Citation: Pieruccioni, D.; Simonetti, M.; Iaccarino, S.; Montomoli, C.; Carosi, R. Microstructural Investigation of Variscan Late-Collisional Granitoids (Asinara Island, NW Sardinia, Italy): New Insights on the Relationship Between Regional Deformation and Magma Emplacement. *Geosciences* **2025**, *15*, 108. https://doi.org/10.3390/geosciences15030108

1. Introduction

Magma emplacement within the continental crust is well documented and modelled in several tectonic settings such as crustal extension [1–7], crustal shortening [8–14], and wrenching [15–27]. Whereas the spatial relationship between the mechanical layering of the crust and the level of magma emplacement is deeply investigated and well described [19,28–30], the correlation between magma emplacement and deformation both

within the magmatic bodies and the host rocks is less described. However, this is of key relevance when dealing with collisional orogens, and particularly the so-called large hot orogens [31], in which partial melting phenomena and magma production with consequent pluton emplacements are common.

The timing of pluton emplacement coupled with field observations of their relationship with host rocks has largely been used as an efficient tool for the temporal (absolute and/or relative) bracketing of regional metamorphism, hydrothermal activity, and deformation in orogenic belts [17,22,32–36]. Therefore, understanding the interplay between deformation, metamorphism, and magmatic processes is a key point to unravelling the complex evolution of the orogens. A close relationship between magma emplacement and deformation has been widely documented all over the world and a close connection between granitic intrusion and deformation has been highlighted in many cases [22,37–45]. Granitoid emplacement can be pre-, syn- or post-tectonic with respect to the regional deformation events. Although nowadays we are all aware of these possibilities, mesoscopic features and field data collected in plutons often seem to suggest, at least at first glance, a post-tectonic emplacement of intrusions since evidence of mesoscale deformation is absent and crosscutting relationship with surrounding rocks occurs. However, in many cases, when such rocks are studied in detail, several microstructural evidence of active deformation can be recognized suggesting that stresses responsible for regional deformation have a major role in controlling the intrusion of magma [39,41–43,46–48].

In this paper, we describe and discuss a variety of deformation-related microstructures observed in quartz, feldspar and mica, developed from sub-magmatic to low-temperature solid-state conditions, within granitoids from the Variscan belt of Asinara Island (NW Sardinia, Italy). The new data presented here are the first steps to unraveling the close relationship between deformation and magmatism in northern Sardinia, and together with literature data from other belt fragments, shedding light on the late stages of the Variscan orogeny.

2. Geological Setting

2.1. Regional Geology

Asinara Island is located in northern Sardinia, where a southern European Variscan belt segment crops out [49–51]. The Variscan orogen was formed due to the Devonian-Carboniferous collision between the Laurentia–Baltica and part of the northern Gondwana or peri-Gondwanian terranes [52–56].

For many years Sardinia Island has been studied because of the lack of a strong Alpine age overprint deformation that makes this sector of the orogen an important locality where investigate the Variscan deformations tectonics [50,57–60].

The Sardinian Variscan basement is divided into three main tectono-metamorphic zones (Figure 1; [50]): (1) the external zone (foreland area, SW Sardinia), consisting of a sedimentary sequence from pre-Cambrian(?)-Cambrian to lower Carboniferous, showing very low-grade metamorphism [61,62]; (2) the nappe zone, subdivided into the external nappe (central to southern Sardinia), deformed mainly under low-grade metamorphic conditions (P = 0.4–0.5 GPa and T = 370–400 °C; [63]), and the internal nappe (northern to central Sardinia) constituted by two metamorphic complexes: the low-grade metamorphic complex (LGMC; P = 0.6–0.8 GPa and T = 420–450 °C; [63]) and the medium-grade metamorphic complex (MGMC); (3) the inner zone, characterized by the migmatitic complex (high-grade metamorphic complex; HGMC) made of migmatites derived from Cambrian(?) micaschist, paragneiss, and Ordovician protoliths (e.g., [64]).

The Posada–Asinara shear zone (PASZ), a nearly 150 km long dextral transpressive shear zone of Variscan age, marks the contact between the MGMC and the HGMC (Figure 1; e.g., [51,58,65–67]).

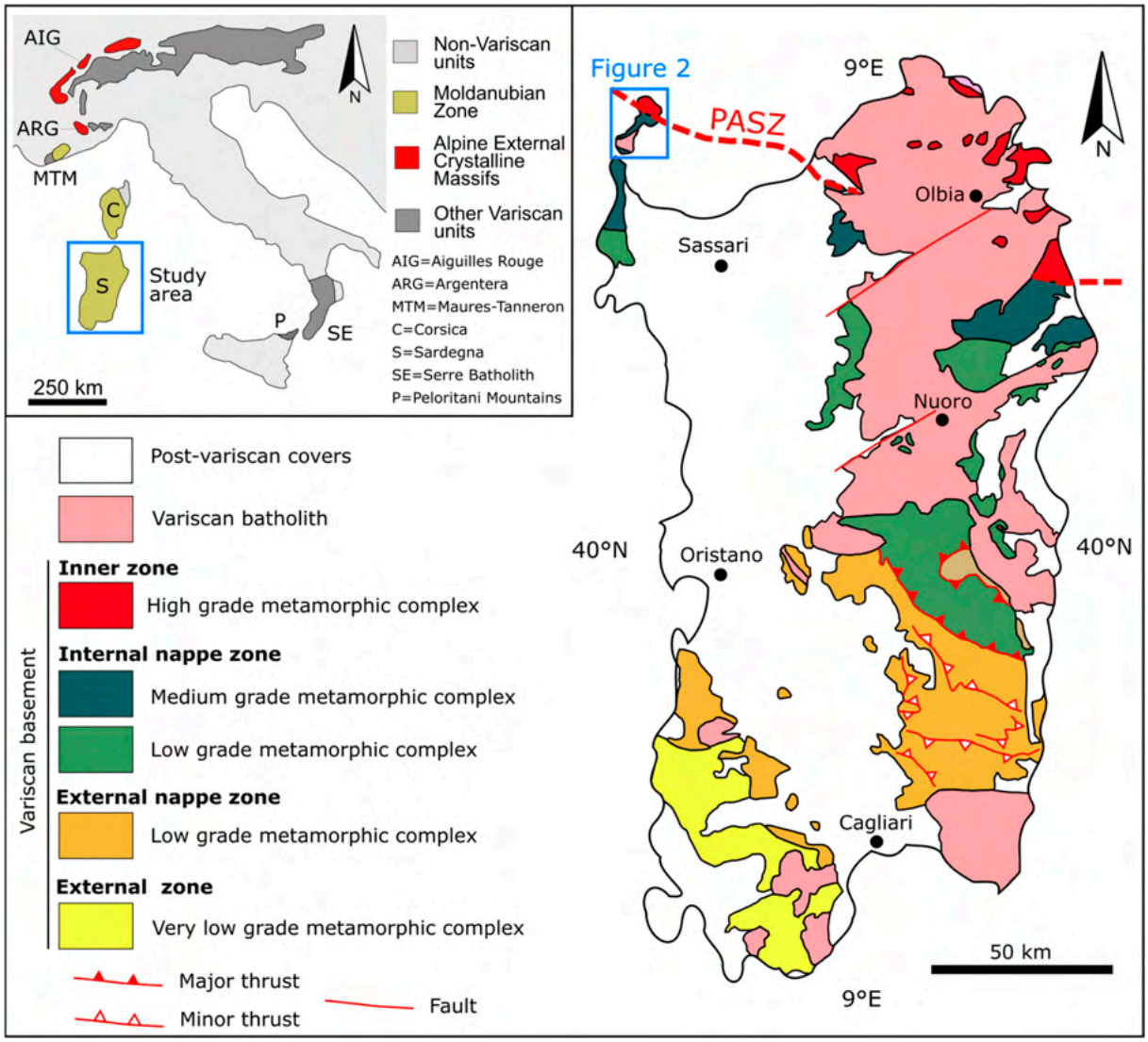

Figure 1. Geological sketch map of the Variscan belt in Sardinia and location of the study area (modified after [50]).

Specifically, Asinara Island represents the north-westernmost part of the Sardinian Variscan belt and is characterized by the transition from the MGMC to the HGMC (Figure 1). This transition is through a zone where prograde Barrovian metamorphic assemblages rapidly change from oligoclase + garnet to garnet + staurolite ± kyanite assemblages moving northward (Figure 2; [68,69]). The P-T conditions of the Barrovian metamorphic stage in the MGMC were estimated by refs. [70,71] at P = 0.8–1.0 GPa and T = 560 °C using classical geothermobarometry on garnet-staurolite micaschist and orthogneiss. Metamorphic conditions of the migmatite of the HGMC were estimated by ref. [71] on amphibolites embedded within them, recognizing an early granulitic stage characterized by P = 0.7–0.8 GPa and T = 720–740 °C. This stage was followed by amphibolite facies equilibration at T = 500–600 °C and P = 0.3–0.4 GPa [68,70] and finally greenschist facies equilibration at T = 451–467 °C and P = 0.27–0.29 GPa [72].

The Posada–Asinara shear zone (PASZ), a nearly 150 km long dextral transpressive shear zone of Variscan age, marks the contact between the MGMC and the HGMC (Figure 1; e.g., [51,58,65–67]).

Specifically, Asinara Island represents the north-westernmost part of the Sardinian Variscan belt and is characterized by the transition from the MGMC to the HGMC (Figure 1). This transition is through a zone where prograde Barrovian metamorphic assemblages rapidly change from oligoclase + garnet to garnet + staurolite ± kyanite assemblages moving northward (Figure 2; [68,69]). The P-T conditions of the Barrovian metamorphic stage in the MGMC were estimated by refs. [70,71] at P = 0.8–1.0 GPa and T = 560 °C using classical geothermobarometry on garnet-staurolite micaschist and orthogneiss. Metamorphic conditions of the migmatite of the HGMC were estimated by ref. [71] on amphibolites embedded within them, recognizing an early granulitic stage characterized by P = 0.7–0.8 GPa and T = 720–740 °C. This stage was followed by amphibolite facies equilibration at T = 500–600 °C and P = 0.3–0.4 GPa [68,70] and finally greenschist facies equilibration at T = 451–467 °C and P = 0.27–0.29 GPa [72].

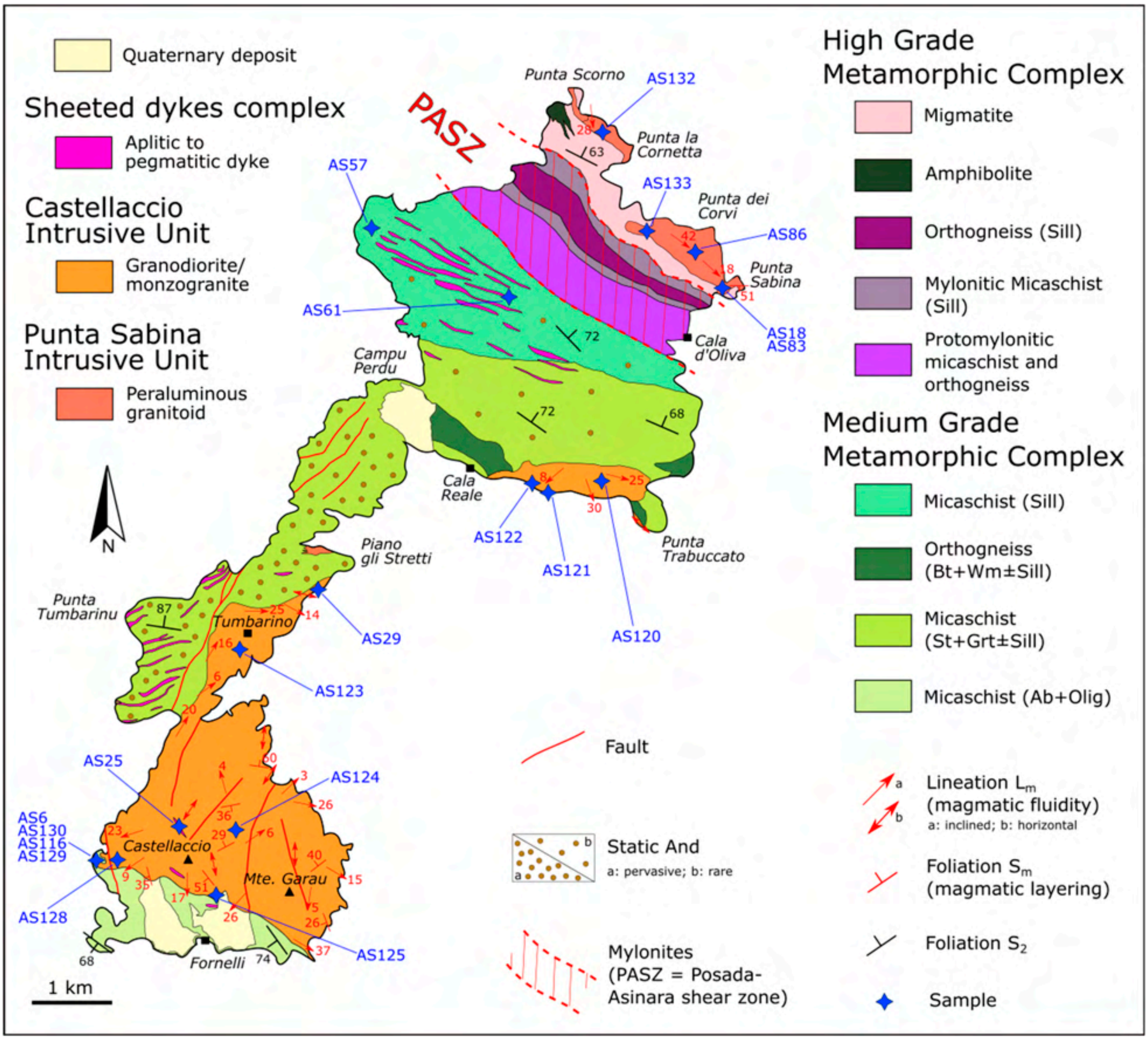

Figure 2. Geological sketch map of Asinara Island and sampling locations (modified after [73,74]).

Four deformation phases are recognized [66,68,73]. The first deformation phase (D_1) is related to collision and thickening; it was associated with HP metamorphism at P ≈ 1.8 GPa and T ≈ 460–500 °C [75,76]. This event is well recorded in the MGMC. Barrovian minerals (chlorite, biotite, garnet, staurolite, kyanite, and sillimanite) started to grow at the end of D_1, locally showing a syn-kinematic growth at the beginning of the second deformation phase (D_2). D_2 is characterized by a transpressive deformation [51] under amphibolite-facies conditions [70]. During this phase, the PASZ started to become active, and the onset of the transpression has been constrained by $^{40}Ar/^{39}Ar$ dating on white mica and U-Th-Pb dating on monazite at ~320–315 Ma [58,77,78]. The activity of the PASZ continued during the D_3 phase under the P-T conditions of shallower crustal level (T ≈ 420–300 °C and P ≈ 0.4–0.2 GPa, as estimated in the Nurra area by ref. [69]). The D_3 is mainly characterized by metric chevron and/or asymmetric folds, associated with an S_3 axial plane crenulation cleavage [58]. The last deformation phase (D_4) developed due to the collapse of the belt, and it is associated with the development of open folds and brittle–ductile shear zones [36,44,79,80].

2.2. Magmatism of Corsica–Sardinia Batholith

The Corsica–Sardinia batholith is a composite 500 km long, 50 km wide plutonic province that resulted from the coalescence of several magmatic events and is continuously exposed from northern Corsica to southeastern Sardinia (Figure 1; [81–84]). Three magmatic suites have been distinguished within this batholith based on field relationships, geochronological data, and geochemical datasets [82,84,85].

The early magmatic sequence (U_1) developed in northwestern Corsica around 345–337 Ma [86] during a compressional event, forming N–S-oriented pluton and subvolcanic complexes [87,88]. U_1 melts gave rise to high-Mg-K calc-alkaline plutons emplaced at depths ranging from mid-crustal levels ($P < 0.37$ GPa; [88]) up to the surface.

The second magmatic suite (U_2) represents the most extended magmatic calc-alkaline sequence exposed in the Corsica–Sardina batholith, developed from 322 to about 285 Ma [44,86,89,90]. The production of melts increased in volumes at around 310–305 Ma, generating large monzogranitic massifs emplaced episodically within NW–SE-oriented shear zones [36,44,45,90].

The last magmatic suit (U_3) is formed by post-orogenic alkaline granites and subvolcanic complexes, developed between about 290 and 260 Ma [83,86,89], and emplaced at very shallow structural levels ($P < 0.2$ GPa).

3. Materials and Methods

Geological mapping and attitude of the main structural elements (i.e., foliations and lineations) were acquired with a traditional approach, integrated with FieldMOVE application by PETEX (Petroleum Experts, https://www.petex.com/pe-geology/move-suite/digital-field-mapping/ accessed on 12 January 2022). The dataset was handled through the open-source software QGIS v3.20.3 (https://www.qgis.org accessed on 1 November 2021). Structural data were processed using Stereonet v11.4.2 (https://www.rickallmendinger.net/stereonet accessed on 25 June 2022), plotted in the lower hemisphere Wulff projection.

During the field survey, 26 specimens of magmatic rocks were collected. In this paper, we deal with a set of 20 thin sections over the entire samples collection, which has been selected for the microstructural study of the three intrusive units (Figure 2): Castellaccio Unit (12 samples), Punta Sabina Unit (5 samples), and the sheeted dykes complex (3 samples). Samples were collected in different parts of the intrusions (close to the contact with the host rocks, in the central part and intermediate positions) to observe possible variations. We acquired high-resolution images of the microstructures by using an Axios Camera (model Axiocam 208 color) mounted on a Leica Microscope (model Leica DRXP), both hosted at the Department of Geological Survey of Italy (Rome). The recrystallization microstructures of the main mineral phases, which gave the temperature range of deformation, are based on studies by refs. [91–94] and references therein.

4. Magmatic Rocks of Asinara Island

In this section we report on the main field and petrographic features of the studied rocks, partly deriving from previous works [68,73,74,95] and integrated by new field and microscopic analysis, to provide the reader with an exhaustive background on the magmatic rocks of Asinara Island.

Based on field data, crosscutting relationships and petrographic data, the magmatic rocks (U_2) of the island are divided into three different units (Figure 2; [74]): (i) Castellaccio intrusive unit; (ii) Punta Sabina intrusive unit; and (iii) sheeted dyke complex. These intrusive units are mainly granitoids intruded into the medium- to high-grade micaschist and paragneiss and within the migmatitic complex (Figure 2) and always crosscut the main metamorphic regional foliation (S_2; Figure 2).

and paragneiss and within the migmatitic complex (Figure 2) and always cross
main metamorphic regional foliation (S_2; Figure 2).

4.1. Field and Petrographic Description

4.1.1. Castellaccio Intrusive Unit

The Castellaccio intrusive unit crops out mainly in the southern part of the isla
between the Forcelli and Franco Stadium areas (Figure 2).

Recent mapping conducted in the CARG Project framework (Italian National Geo
logical Mapping Project at 1:50,000 scale) revealed that the granite cropping out near Pia
Reale (Figure 2) is also part of the Castellaccio Intrusive Unit because it p
the same features as the main outcrop. This unit consists of inequigranular g
monzogranite characterized by large idiomorphic K-feldspar phenocrysts, which often
some cases, a magmatic foliation is also locally developed (Figure 3A).

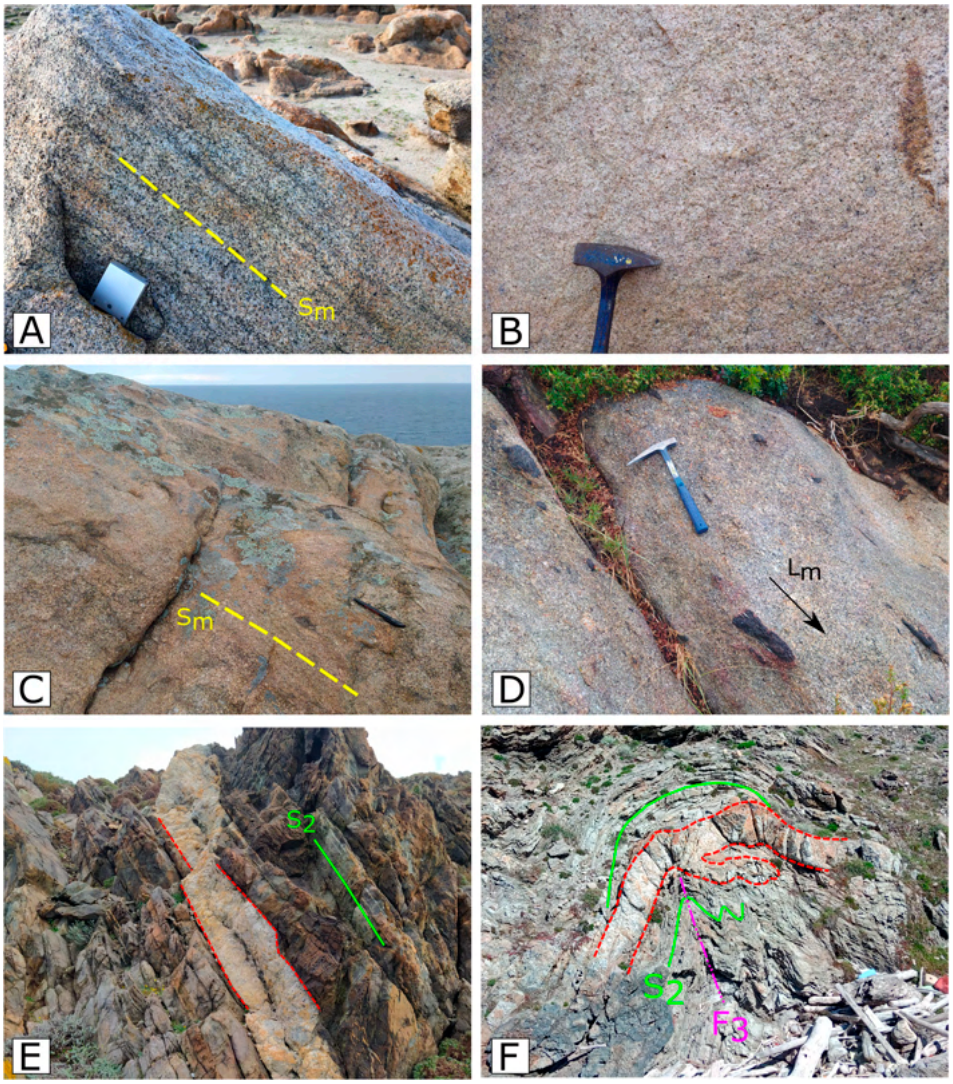

Figure 3. (**A**) magmatic layering (S_m) in the Castellaccio intrusive unit; (**B**) muscovite ± garn
bearing microleucomonzogranite that crops out between the Castellaccio intrusive unit and the host
rock; (**C**) magmatic layering (S_m) in the Punta Sabina intrusive unit; (**D**) magmatic lineat
marked by stretched xenoliths of migmatite and small crystals of K-feldspars; (**E**) aplitic to pegmatitic
dyke intruded along the main foliation S_2; (**F**) aplitic to pegmatitic dyke intruded along the main
foliation S_2 mimicking the F_3 fold.

This foliation is mainly determined by the (001) plane of the biotite, muscovite and K-feldspar, and its orientation shows a general sub-horizontal or weakly inclined towards the E-SE (Figure 4A) attitude, which is discordant with respect to the main fabric of the host rocks (S_2; Figure 2). Large K-feldspar phenocrystals together with mafic enclaves and

This foliation is mainly determined by the (001) plane of the biotite, muscovite and K-feldspar, and its orientation shows a general sub-horizontal or weakly inclined towards the E-SE (Figure 4A) attitude, which is discordant with respect to the main fabric of the host rocks (S_2; Figure 2). Large K-feldspar phenocrystals together with mafic enclaves and metamorphic xenoliths, are often aligned forming an object lineation of primary origin. This lineation has an overall centrifugal orientation with respect to the main body of the intrusion and a slightly medium (50°) inclination (Figure 4B).

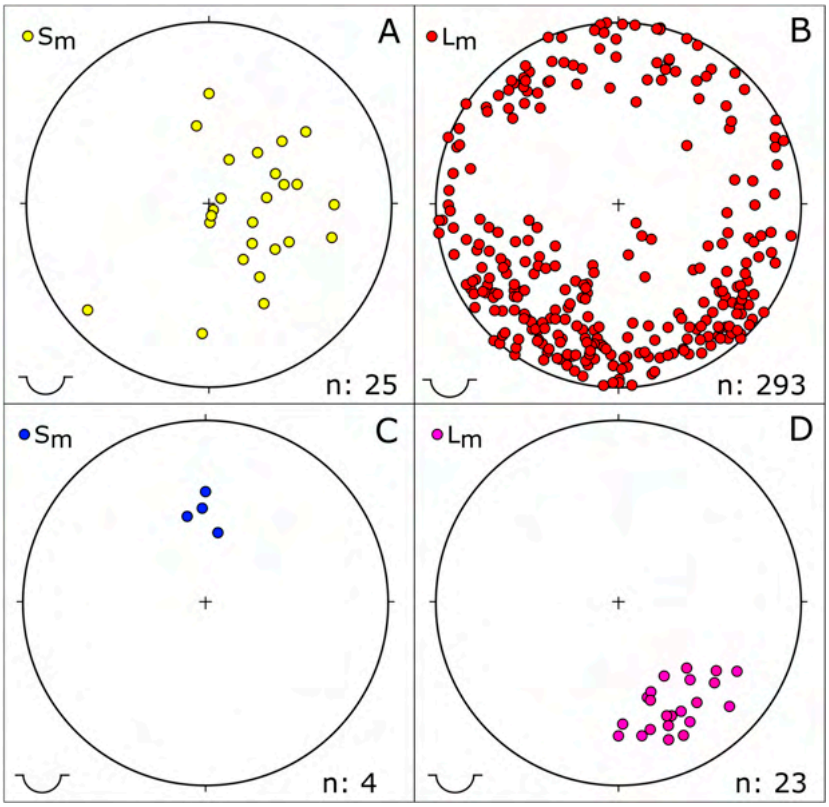

Figure 4. Equal-angle, lower hemisphere projections of the main structural elements measured in the magmatic rocks: (**A**) magmatic layering in the Castellaccio intrusive unit; (**B**) magmatic lineation in the Castellaccio intrusive unit; (**C**) magmatic layering in the Punta Sabina intrusive unit; (**D**) magmatic lineation in the Punta Sabina intrusive unit.

The contacts between the granite units and the metamorphic rocks along the southern and south-eastern margins of the pluton are mostly characterized by a thick, continuous, belt of microleucomonzogranite that reaches a maximum thickness of about 20–30 m [95]. These rocks show distinctive features typical of quenched melts, such as very-fine grain size (0.5–2 mm), globular quartz aggregates, and rare to absent K-feldspar phenocrysts (Figure 3B). These observations are broadly consistent with the occurrence of diffuse micropegmatite pockets and metamorphic xenoliths along the southern margin of the intrusion.

The main mineralogy comprises quartz, K-feldspar, plagioclase, muscovite, and biotite, while accessory minerals are apatite, zircon and opaque minerals. A typical feature of these rocks is the presence of large K-feldspar phenocrysts with a variable size between 3 cm and 20 cm. Taking into account the size and the abundance of large idiomorphic K-feldspar phenocrysts, within the Castellaccio intrusion several subdivisions have been made by refs. [73,95]: (i) the M.te Garau Unit, consisting of fine-grained leucomonzogranite with diffuse micropegmatitic pockets; (ii) the Scalpellini Unit, that is a fine-grained leucomonzogranite or leucogranodiorite with rare small (1–3 cm) K-feldspar phenocrysts; (iii) the Castellaccio Unit, consisting in medium-grained granodiorite with abundant and large (3–10 cm) K-feldspar phenocrysts; (iv) the Tumbarino Unit, that is represented by coarse-grained granodiorite with K-feldspar megacrysts up to 20 cm in size, K-feldspar-rich cumulates, and abundant microgranular mafic enclaves.

The Castellaccio Unit emplaced at P = 0.20–0.25 GPa, was recently dated by U-(Th)-Pb on monazite and zircon at 320–310 Ma [96].

4.1.2. Punta Sabina Intrusive Unit

The Punta Sabina Unit crops out in the northern part of the island, forming a large body between Punta Sabina—Punta dei Corvi and a second minor body between Punta Scorno—Punta la Cornetta (Figure 2). Overall, the geometry of both bodies is consistent with that of a stretched oblate ellipsoid, interpreted as a part of a NW-SE elongated sill-like body (Figure 2). This unit consists of peraluminous granitoid with stromatic enclaves [68], and the main mineralogy comprises quartz, plagioclase, K-feldspar, muscovite, and biotite. Accessory minerals are apatite, zircon and rare opaque minerals. A local magmatic foliation, dipping at a medium angle toward the S (Figures 3C and 4C), is recognized. Rare large idiomorphic K-feldspar crystals, with subordinate mafic enclaves and metamorphic xenoliths, are often aligned forming an object lineation of primary origin, plunging at a shallow to medium angle toward the SE (Figures 3D and 4D).

4.1.3. Sheeted Dyke Complex

The sheeted dyke complex is the third intrusive unit recognized in the studied area, and it mainly crops out in the western and northwestern parts of the island (Figure 2). It consists of peraluminous microleucogranite and pegmatite with extremely variable composition and field appearance, ranging from aplitic to pegmatitic texture. This textural variation is also visible within single dykes where a transition from aplite to pegmatite can be observed from the edge to the center, or vice versa (Figure 3E). Their thickness varies from decimetric to plurimetric, with important lateral continuity reaching several tens of meters. Frequently, dykes are interconnected, forming complex networks. They are discordant, or locally para-concordant (Figure 3E), with respect to the S_2 foliation of the host rocks. In some cases, the dykes mimic the fold structures intruding along the S_2 foliation (Figure 3F), but at a closer look, they appear discordant.

The main mineralogy is composed of quartz, feldspar, muscovite and biotite. Portions enriched in tourmaline and/or garnet are sporadically recognized, while accessory minerals are apatite, zircon, opaque minerals and allanite [68].

4.2. Microstructural Data

The studied rocks display a magmatic texture, with euhedral to subhedral micas and plagioclase, subhedral to anhedral K-feldspar and anhedral quartz, without mesoscopic evidence of deformation. Nevertheless, all the granitoids exhibit, at different extents, several deformation microstructures evident at the thin-section scale.

4.2.1. Castellaccio Intrusive Unit

The most striking evidence of the granitoids of the Castellaccio intrusive unit is represented by chessboard pattern extinctions in quartz (Figure 5A), resulting from the combined activation of basal <a> and prism <c> slip systems [97,98], which is mostly referred to occur at T above 650 °C for pressure up to 1.0 GPa [91–93,99].

Sub-solidus high-temperature deformation comes from grain boundary migration (GBM) recrystallization [91–93] of quartz crystals (T 500–700 °C) with examples of inequigranular grain size and interlobate and sutured crystals boundaries (Figure 5B). Sometimes feldspar shows a bimodal grain size evidenced by the presence of sub-grains and small new grains around larger grains (Figure 5C). This evidences recrystallization by subgrain rotation dynamic recrystallization (SGR; [100–104]). Moreover, the high- to medium-temperatures deformation (450–600 °C) is evidenced by a few examples of myrmekitic intergrowths between quartz and plagioclase (Figure 5D; [92,105]), and by a small recrystal-

small new grains around larger grains (Figure 5C). This evidences recrystallization by sub-grain rotation dynamic recrystallization (SGR; [100–104]). Moreover, the high- to medium-temperatures deformation (450–600 °C) is evidenced by a few examples of myrmekitic intergrowths between quartz and plagioclase (Figure 5D; [92,105]), and by a small recrystallized grain along feldspar grain boundaries that are indicative of bulging recrystallization (BLG; [92,106,107]).

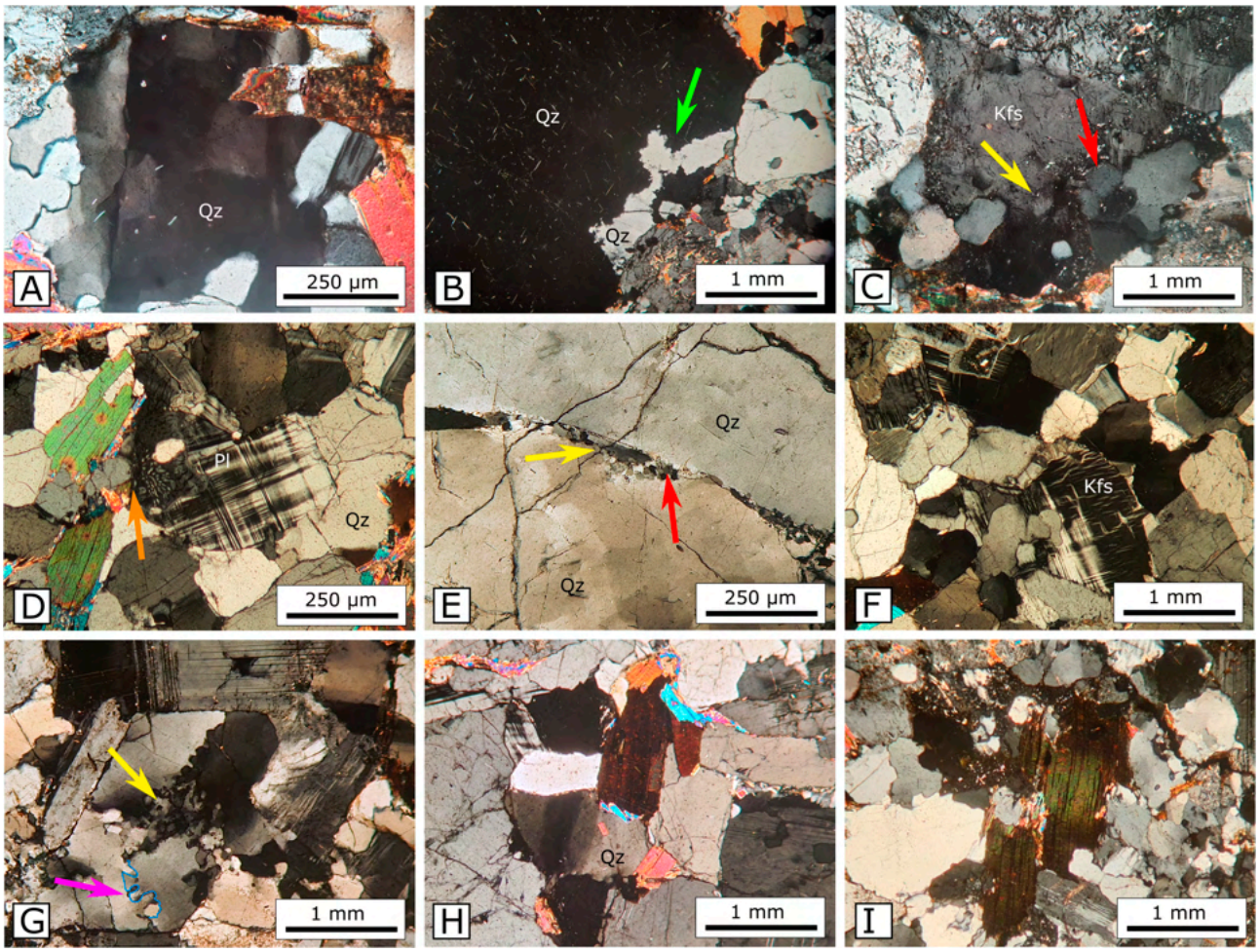

Figure 5. Microstructures of the Castellaccio intrusive unit: (**A**) chessboard pattern extinction in quartz crystal; (**B**) lobate grain boundary (green arrow) indicative of GBM in quartz grain; (**C**) new grains (red arrow) and sub-grains (yellow arrow) indicative of SGR in feldspar crystal; (**D**) myrmekites (cites orange arrow) around plagioclase crystal; (**E**) bimodal grain size with new grains (red arrow) and sub-grains (yellow arrow) indicative of SGR in quartz; (**F**) deformation lamellae and flame perthites in K-feldspar; (**G**) quartz grain with evident overprinting relationship between GBM (green line), SGR (yellow arrow) and BLG (pink arrow); (**H**) undulate extinction in quartz grain; (**I**) undulate extinction in biotite crystal. Mineral abbreviations according to [108].

In many samples, it is common to recognize places where quartz shows a bimodal grain size where sub-grains and small new grains are present surrounding larger grains (Figure 5E). This feature provides evidence of quartz recrystallization by sub-grain rotation dynamic recrystallization (SGR), indicative of a temperature of deformation ranging between 400 and 500 °C [91–93,109]. Rarely, quartz forms a core-and-mantle structure. In this range of temperature feldspar still deforms mainly by internal microfracturing but is assisted by minor dislocation glide [93,110,111], producing bent twins, undulate extinction, deformation bands and kink bands with sharp boundaries (Figure 5F). Perthite with tapering "flame-shaped" albite lamellae (flame perthite) are locally present in K-feldspar, especially at grain boundaries and high-strain sites (Figure 5F; e.g., [93,112,113]).

Low-temperature deformation microstructures in quartz crystals, produced at $T \leq 400$ °C, are undulate extinction and deformation lamellae, caused by dislocation glide and creep on basal glide planes in the (c) <a> direction [93,114–117]. Under these condi-

tions, a dominant dynamic recrystallization mechanism is BLG recrystallization in quartz crystals overprinting previous microstructures (Figure 5G; [91,92]). Other microstructures here observed, mainly consisting of undulate extinction in quartz (Figure 5H) and biotite (Figure 5I), developed probably at temperatures ranging from 250 to 400 °C [92,118–121].

4.2.2. Punta Sabina Intrusive Unit

The rocks belonging to the Punta Sabina Unit show chessboard extinction in quartz crystals (Figure 6A; [91,97,98]) indicating a temperature of deformation above 650 °C—e.g., [99], happened under sub-magmatic conditions. Deformation at the same T conditions is supported by rare sub-magmatic fracture in feldspars (Figure 6B), indicating deformation in the presence of melt and well-documented in other late-Variscan granitoids — e.g., [44,45,47]. These microstructures are typical of rigid or semi-rigid crystals, where a melted fraction still occurs and late magmatic crystals grow in fractures breaking apart early crystallized minerals—e.g., [122]. In the studied rock samples, medium- to fine-grained interstitial quartz crystallizes within veins propagating into large, fractured feldspar, consistently with melt migration into dilatation sites. In places, feldspar shows evidence of recrystallization by sub-grain rotation dynamic recrystallization (SGR; Figure 6C; [100–104]). Quartz grain boundary migration (GBM) recrystallization (Figure 6A), indicating a temperature of deformation between 500 and 700 °C [91,92], supports the occurrence of solid-state high-temperature deformation.

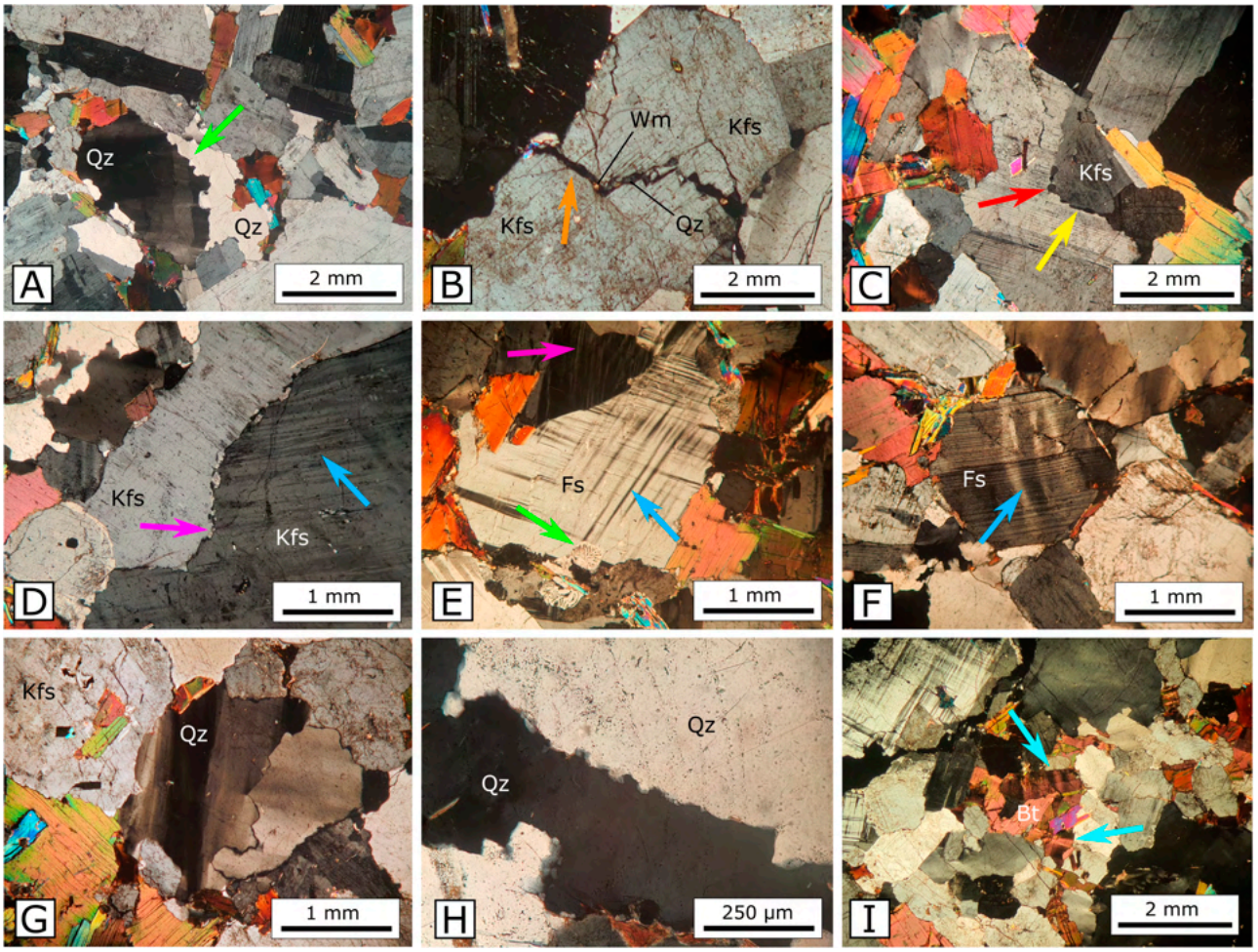

Figure 6. Microstructures of the Punta Sabina intrusive unit: (**A**) quartz grain with lobate grain boundary (green arrow) indicative of GBM and quartz crystal with chessboard pattern extinction; (**B**) sub-magmatic fracture (orange arrow) in K-feldspar filled with quartz and white mica; (**C**) K-feldspar grain with evident sub-grains (yellow arrow) and new grains (red arrow) indicative of SGR; (**D**) large K-feldspar grains showing BLG recrystallization (pink arrow) and deformation lamellae (blue arrow); (**E**) myrmekite between the grain boundaries of feldspar and quartz crystals (green arrow). Deformation lamellae (blue arrow) and flame perthites (pink arrow) in feldspar; (**F**) feldspar grain with kink bands (blue arrow); (**G**) undulate extinction in quartz grain; (**H**) BLG recrystalliza-

(**B**) sub-magmatic fracture (orange arrow) in K-feldspar filled with quartz and white mica; (**C**) K-feldspar grain with evident sub-grains (yellow arrow) and new grains (red arrow) indicative of SGR; (**D**) large K-feldspar grains showing BLG recrystallization (pink arrow) and deformation lamellae (blue arrow); (**E**) myrmekite between the grain boundaries of feldspar and quartz crystals (green arrow). Deformation lamellae (blue arrow) and flame perthites (pink arrow) in feldspar; (**F**) feldspar grain with kink bands (blue arrow); (**G**) undulate extinction in quartz grain; (**H**) BLG recrystallization in quartz grains; (**I**) biotite crystals with kink bands (bright blue arrow). Mineral abbreviations according to [108].

At deformation temperatures between 450 °C and 600 °C dislocation climb becomes possible in feldspar [92,106,107] and recrystallization starts to be important, occurring mainly by bulging (Figure 6D). Moreover, microstructures in this temperature interval are represented by a few examples of myrmekite between the grain boundaries of feldspar and quartz crystals (Figure 6E; [92,105]). The bimodal grain size of quartz crystals, where sub-grains and small new grains are present surrounding bigger grains overprinting on interlobate and sutured crystals boundaries provided by GBM are frequently observed. This microstructure is caused by recrystallization by sub-grain rotation dynamic recrystallization (SGR), which takes place between 400 and 500 °C [91–93,109]. Feldspar microstructures related to this temperature interval are provided by internal microfracturing assisted by minor dislocation glide [92,110,111], producing bent twins, undulate extinction, deformation bands and kink bands with sharp boundaries (Figure 6F), while K-feldspar shows flame perthite (Figure 6E; e.g., [92,112,113]).

Sub-solidus low-temperature deformation microstructures in quartz crystals are provided by dislocation glide and creep [92,114–117], producing undulate extinction (Figure 6G) and deformation lamellae, indicating a temperature of deformation below 450 °C. Under these conditions BLG recrystallization in quartz crystals becomes dominant (Figure 6H; [91–93]). Undulate extinction and kink bands frequently occur in mica crystals (Figure 6I), pointing to intracrystalline plastic deformation at temperatures between 250 and 400 °C [92,118–121].

4.2.3. Sheeted Dyke Complex

The rocks of this intrusive unit are felsic aplitic to pegmatitic dykes. They are poorly studied in Asinara Island and future investigations are needed. Preliminary observations show extremely variable microstructures passing from moderately deformed (sample AS57; Figure 2) to undeformed rocks (sample AS25; Figure 2).

Chessboard pattern extinctions in quartz (Figure 7A; [91–94,99]), mainly observed in sample AS57 and subordinately in sample AS61, suggest sub-magmatic deformation conditions. Although less frequently than in the previously described two intrusive units, sub-solidus high-temperature (500–700 °C) deformation microstructures are provided by quartz GBM recrystallization (Figure 7B; [92–94]). Myrmekitic intergrowths between quartz and plagioclase, indicating a deformation temperature of 450–600 °C [93,105], have been observed only in the sample AS57 (Figure 7C). Moreover, in this range of temperature, there are frequently bent twins, undulate extinction, deformation and kink bands with sharp boundaries are frequent in plagioclase crystals (Figure 7C,D), pointing to internal microfracturing assisted by dislocation glide [93,110,111]. Flame perthites are locally present in K-feldspar—e.g., [93,112,113].

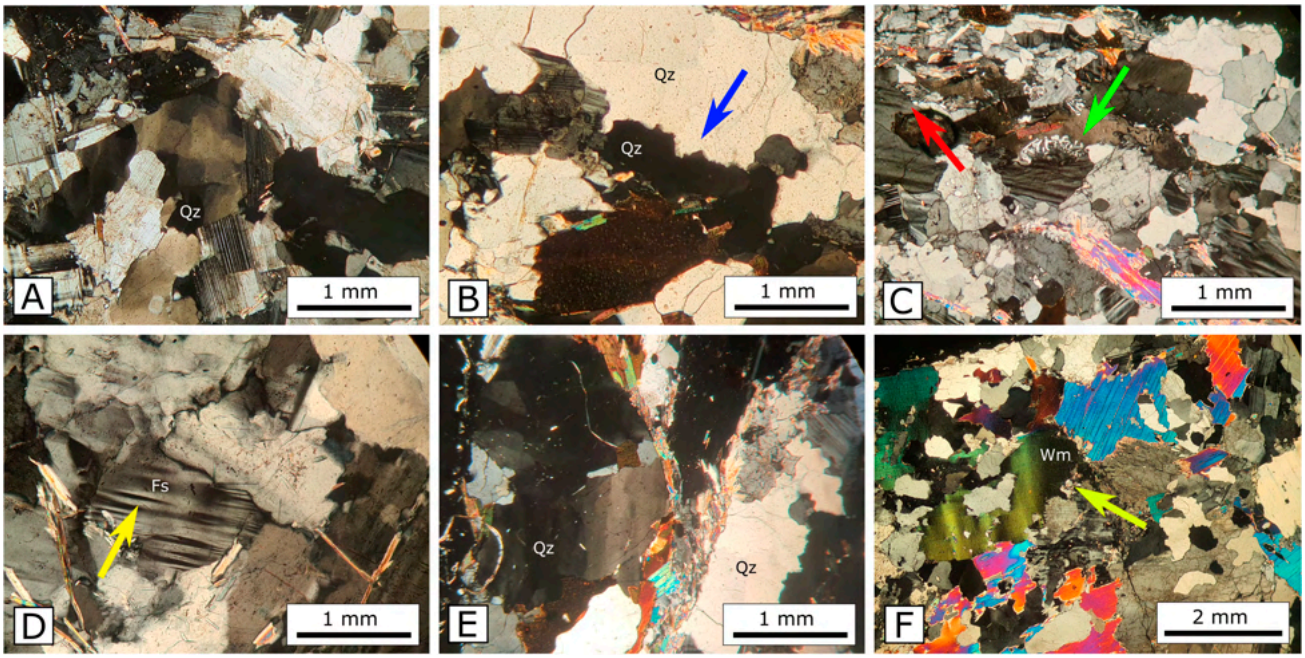

Figure 7. Microstructures of sheeted dyke complex. (**A**) chessboard pattern extinction in quartz crystal; (**B**) lobate grain boundary (blue arrow) indicative of GBM in quartz grain; (**C**) myrmekites (green arrow) and deformation lamellae (red arrow) in feldspars; (**D**) deformation lamellae (yellow arrow) in feldspar grain; (**E**) undulate extinction in quartz grain; (**F**) undulate extinction in white mica grain (yellow arrow). Mineral abbreviations according to [108].

5. Discussion

Asinara Island is an important place for studying the architecture and the processes that occurred in a key sector of the Variscan belt, namely the transition between the nappe zone and the internal zone. Despite this, available investigations are scarce because of the former access restrictions, which lasted for many years, and limited access to the island, and only recently a modern geological map of the whole island [73] has been published.

Although the structural, metamorphic and tectonic evolution of this belt sector is largely delineated and widely accepted, the granitoids of Asinara Island were not properly studied in detail, especially from the structural point of view. An attempt to better describe the structural evolution of the Castellaccio intrusive unit has been made by ref. [95].

Magmatic rocks of Asinara Island are generally interpreted as late- to post-Variscan intrusions characterized by a post-tectonic emplacement at the end of the tectonic evolution of the belt. Recently, the magmatic rocks of the island were grouped into three intrusive units [74]. Field data show that igneous rocks crosscut the regional S_2 foliation, suggesting a post-tectonic emplacement with respect to the D_2 phase which is the main deformation phase recorded by the country metamorphic rock. Indeed, in the Castellaccio intrusive unit, the orientation of the magmatic layering is discordant compared to the D_2 and D_3 foliations occurring in the host rocks since it is generally sub-horizontal or dipping at a medium angle and it shows a moderate dispersion (Figure 4A) suggesting a dome-like shape at the scale of the whole pluton. The magmatic lineation shows a centrifugal dispersion (Figure 4B).

intrusive unit, the orientation of the magmatic layering is discordant compared to the D_2 and D_3 foliations occurring in the host rocks since it is generally sub-horizontal or dipping at a medium angle and it shows a moderate dispersion (Figure 4A) suggesting a dome-like shape at the scale of the whole pluton. The magmatic lineation shows a centrifugal dispersion (Figure 4B). Those features are likely to be interpreted as due to the dome shape of the pluton and can be related to the emplacement of the Castellaccio intrusion.

The situation of the Punta Sabina unit is slightly different. This intrusion in some places shows crosscutting relations with S_2 foliation in the host rock but the magmatic lineation is not dispersed. It presents a constant plunging at a medium angle toward the SE (Figure 4D) while the magmatic layering strikes E-W and dips at a medium angle toward the S (Figure 4C) therefore showing a similar orientation to both S_2, with which it forms a small angle, and D_3 structures. Therefore, considering the NW-SE elongated shape of this intrusion and its proximity to the PASZ, a relationship between its emplacement and the late D_2 or D_3 phase (i.e., the transpressional deformation) cannot be excluded. Despite this, it is worth noting that neither the Castellaccio intrusive unit nor the Punta Sabina intrusive unit has evidence of a macroscopic tectonic fabric observed in the field.

However, the detailed microstructural analysis conducted in this work revealed that the studied intrusive units have suffered tectonic stresses that occurred during the cooling of magmatic bodies, inducing both dynamic recrystallization and crystal deformation (Figure 8).

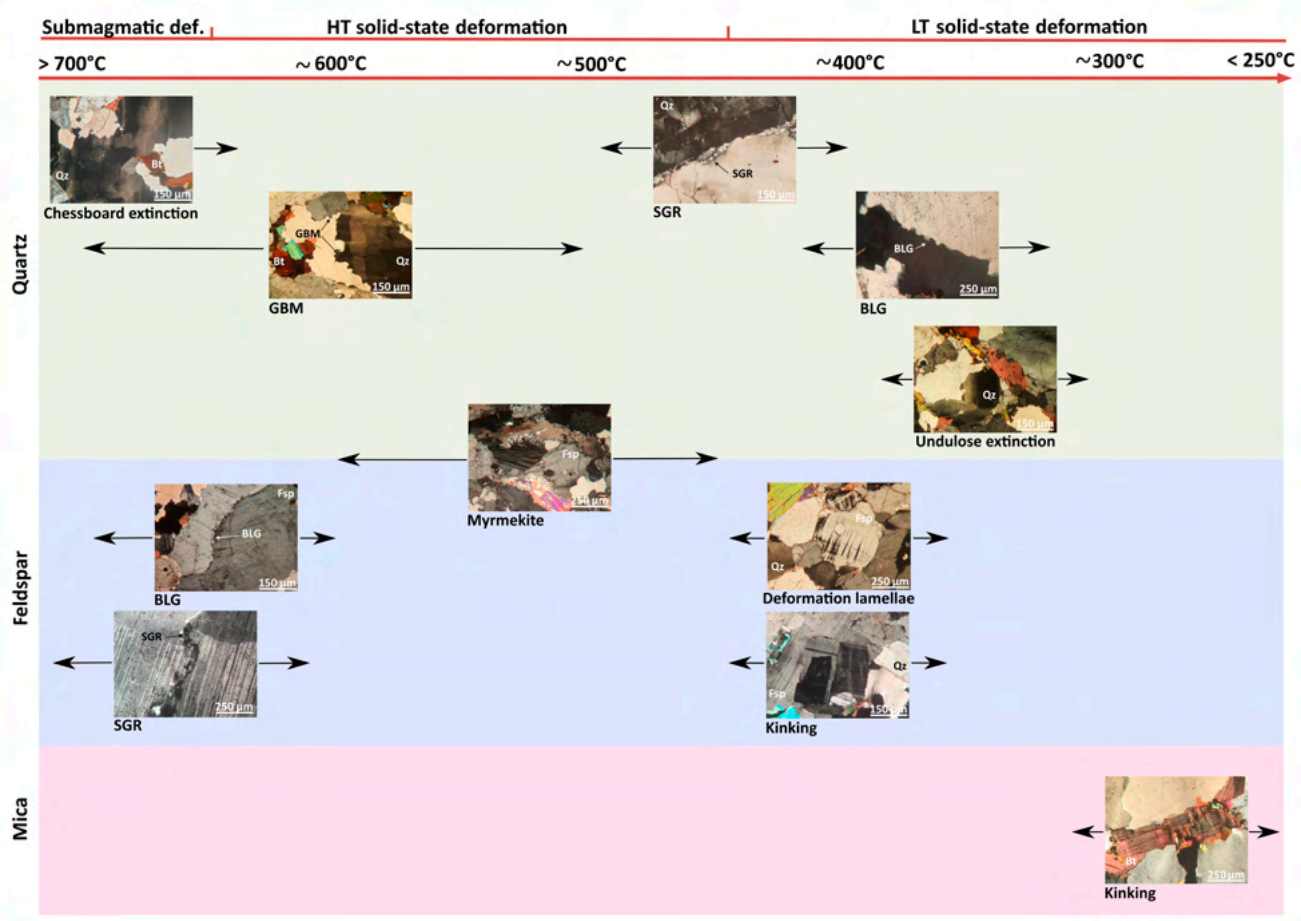

Figure 8. Sub-magmatic to solid-state thermal ranges of deformation mechanisms and associated microstructures for quartz, feldspar and mica grains recognized in the studied granitoid rocks. Temperature ranges (indicated by black arrows) estimated after [91–94]. Mineral abbreviations according to [108].

The Castellaccio and Punta Sabina intrusive units show comparable microstructural features, with a wide range of deformative microstructures, from sub-magmatic to low-temperature sub-solidus conditions — e.g., [91–94] (Figure 8). Rocks belonging to the sheeted dyke complex show extremely variable microstructures (Figure 7), indicative of a

The Castellaccio and Punta Sabina intrusive units show comparable microstructural features, with a wide range of deformative microstructures, from sub-magmatic to low-temperature sub-solidus conditions — e.g., [91–94] (Figure 8). Rocks belonging to the sheeted dyke complex show extremely variable microstructures (Figure 7), indicative of a variation from moderately deformed and recrystallized rocks, such as the other magmatic rocks of the other intrusive units, to completely undeformed (and not recrystallized) rocks.

The main observed microstructures are represented by chessboard extinction and GBM in quartz, whereas feldspar shows sub-magmatic fracture, SGR, BLG, deformation lamellae and myrmekites. These microstructures indicate dynamic recrystallization and deformation at high-temperature conditions (T > 600 °C) that can be linked to a sub-magmatic environment. Evidence of solid-state, medium–high-temperature deformations (T > 450 °C) are provided by deformation lamellae and kinking in feldspar, and by SGR in quartz, partially overprinting GBM microstructures. Finally, low-temperature sub-solidus microstructures (T ⩽ 450 °C) consisting of BLG in quartz and kinking of mica are reported.

This complete sequence of deformation-induced recrystallization and microstructures, operating from sub-magmatic to low-temperature sub-solidus conditions, suggests for all three intrusive units (except for undeformed dykes), an emplacement where deformation was still active, associated with a progressive temperature decrease during the magmatic cooling.

Even if, at the moment, high-resolution geochronological constraints for all the granitic rocks in the northern part of the island, including the dykes are not available in the literature, the Castellaccio intrusive unit was classically considered a post-collisional intrusion. This interpretation was extended by similarity to all the magmatic rocks of Asinara Island and the other sectors of Sardinia—e.g., [44,45]. Recently, the Castellaccio intrusive unit has been dated by U-(Th)-Pb on monazite and zircon at 320–310 Ma [96]. Interestingly, these ages are in the same range of time of the widespread transpressional deformation affecting the whole southern part of the Variscan belt in Europe (Figure 9).

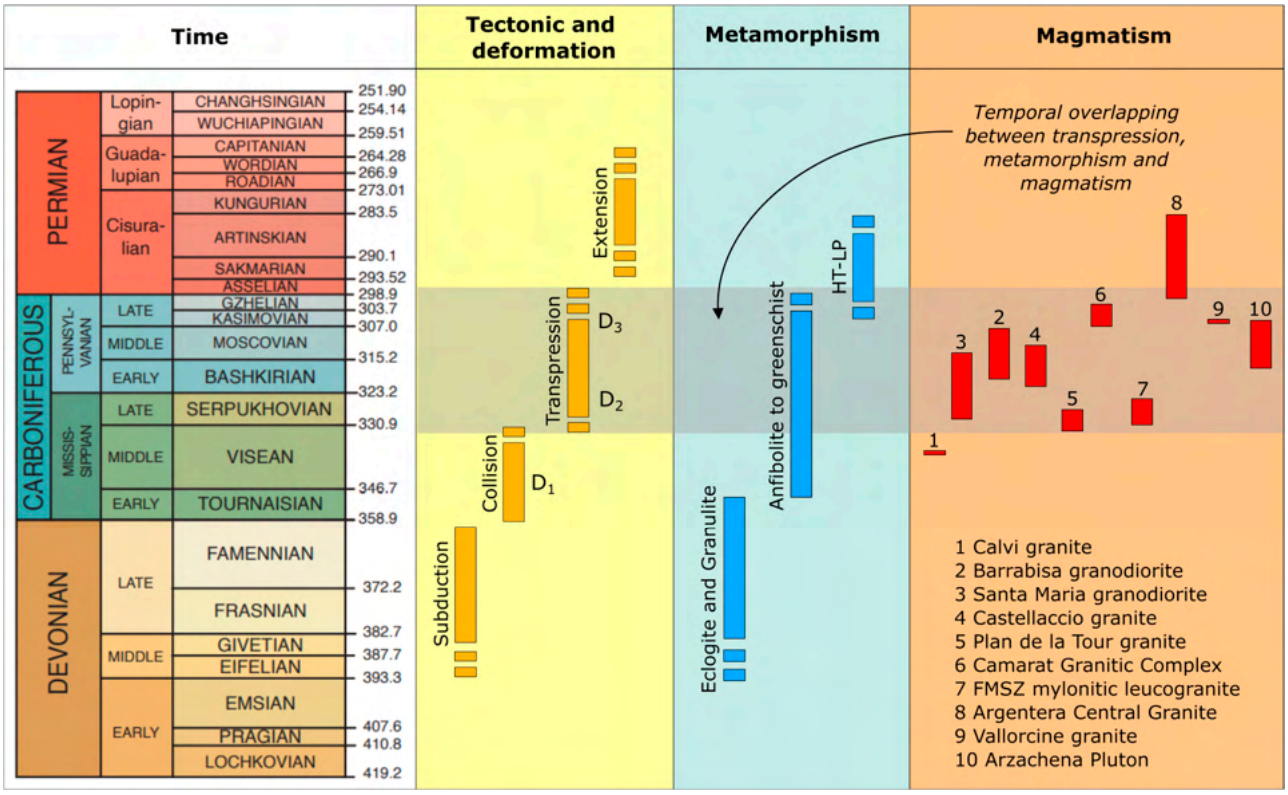

Figure 9. Synoptic table showing the temporal overlapping between tectonic events, main deformation phases, metamorphism and magmatism in the southern Variscides (modified from [59]). The age of magmatism derived from: Calvi granite [86]; Barrabisa and Santa Maria granodiorites [90];

Figure 9. Synoptic table showing the temporal overlapping between tectonic events, main deformation phases, metamorphism and magmatism in the southern Variscides (modified from [59]). The age of magmatism derived from: Calvi granite [86]; Barrabisa and Santa Maria granodiorites [90]; Castellaccio granite [96]; Plan de la Tour granite [123]; Camarat granitic complex [124]; FMSZ mylonitic leucogranite [125]; Argentera central granite [126]; Vallorcine granite [127]; Arzachena pluton [44]. The red rectangle indicates age together with relative error.

Castellaccio granite [96]; Plan de la Tour granite [123]; Camarat granitic complex [124]; FMSZ mylonitic leucogranite [125]; Argentera central granite [126]; Vallorcine granite [127]; Arzachena pluton [44]. The red rectangle indicates age together with relative error.

that is linked to the formation of the east Variscan shear zone network (Figure 10; EVSZ; [53,67,128,129]) This network includes the PASZ with dextral top-to-SE shear sense (Figure 10) [51,58,129–131]. The onset of transpression in northern Sardinia has been well-constrained thanks to U-Th-Pb monazite petrochronology at ~325 Ma [58,78] and by $^{40}Ar/^{39}Ar$ dating [77]. The Asinara Island transpression is expressed by the D_2 and D_3 deformation phases [68] (Figure 9).

That is linked to the formation of the east Variscan shear zone network (Figure 10; EVSZ; [53,67,128,129]) This network includes the PASZ with dextral top-to-SE shear sense (Figure 10) [51,58,129–131]. The onset of transpression in northern Sardinia has been well-constrained thanks to U-Th-Pb monazite petrochronology at ~325 Ma [58,78] and by $^{40}Ar/^{39}Ar$ dating [77]. The Asinara Island transpression is expressed by the D_2 and D_3 deformation phases [68] (Figure 9).

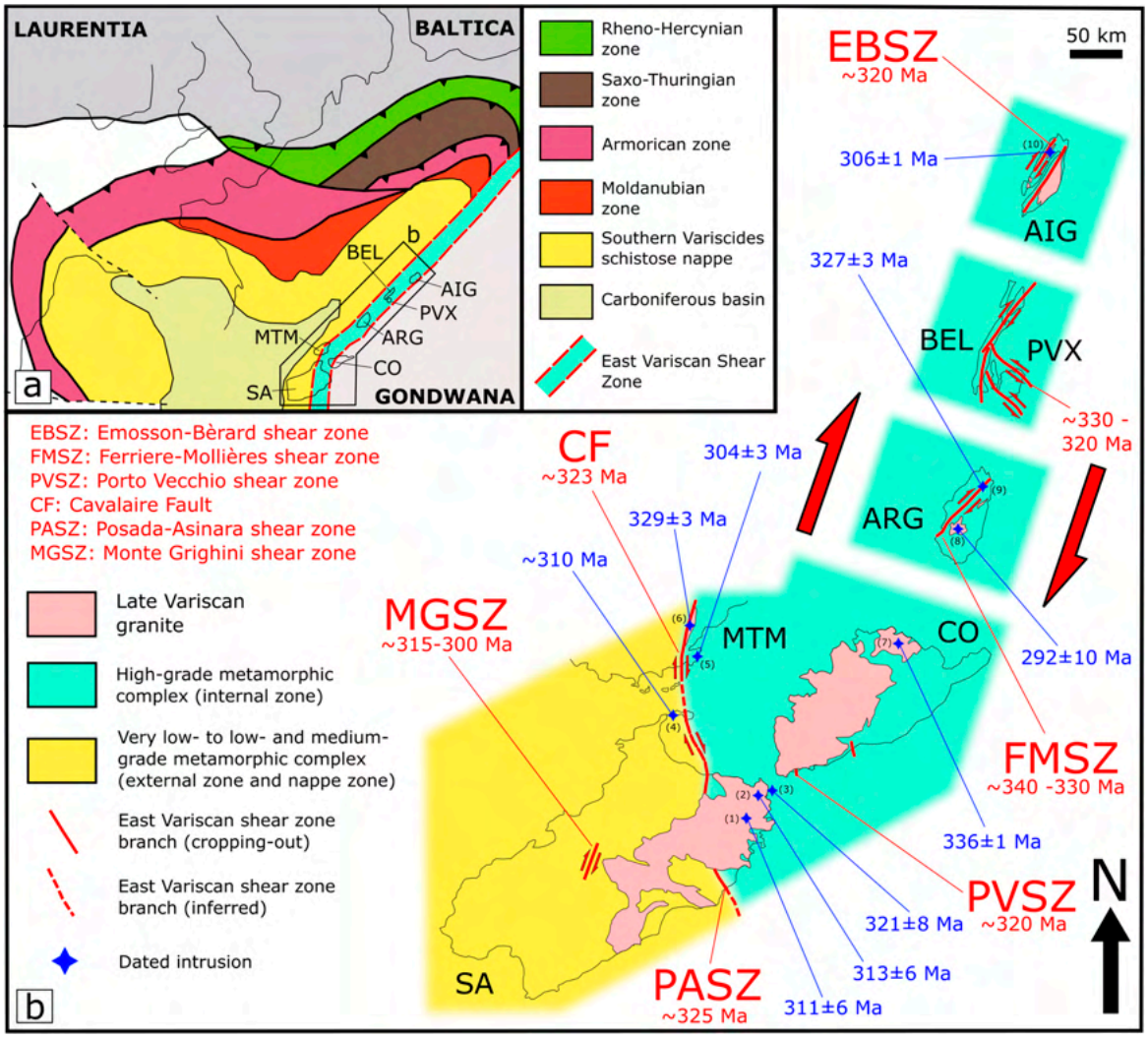

Figure 10. (**a**) Simplified sketch map of the southern European Variscides during the late Carboniferous (modified after [78,121,132]); (**b**) inferred lateral relationship between the Corsica-Sardinia block, the Maures–Tanneron Massif, the Argentera Massif, the Aiguilles Rouges Massif and the Belledonne–Pelvoux Massif (modified after [130]). The age of magmatism derived from: (1) Arzachena Pluton [44]; (2) Barrabisa granodiorite [90]; (3) Santa Maria granodiorite [90]; (4) Castellaccio granite [96]; (5) Camarat granitic complex [124]; (6) Plan de la Tour granite [123]; (7) Calvi granite [86]; (8) Argentera central granite [126]; (9) FMSZ mylonitic leucogranite [125]; (10) Vallorcine granite [127]. Ages of transpression are from [131,133] for the Argentera Massif; [130] for the Aiguilles Rouge Massif; [134] for the Pelvoux Massif; [129] for the Maures–Tanneron Massif; [58,77,78] for the northern Sardinia; [135] for Corsica. Abbreviations: SA—Sardinia; CO—Corsica; MTM—Maures–Tanneron Massif; ARG—Argenterea Massif; PVX—Pelvoux Massif; BEL—Belledonne Massif; AIG—Aiguilles Rouges Massif.

Figure 10. (**a**) Simplified sketch map of the southern European Variscides during the late Carboniferous (modified after [78,121,132]); (**b**) inferred lateral relationship between the Corsica-Sardinia block, the Maures–Tanneron Massif, the Argentera Massif, the Aiguilles Rouges Massif and the Belledonne–Pelvoux Massif (modified after [130]). The age of magmatism derived from: (1) Arzachena Pluton [44]; (2) Barrabisa granodiorite [90]; (3) Santa Maria granodiorite [90]; (4) Castellaccio granite [96]; (5) Camarat granitic complex [124]; (6) Plan de la Tour granite [123]; (7) Calvi granite [86]; (8) Argentera central granite [126]; (9) FMSZ mylonitic leucogranite [125]; (10) Vallorcine granite [127]. Ages of transpression are from [131,133] for the Argentera Massif; [130] for the Aiguilles Rouge Massif; [134] for the Pelvoux Massif; [129] for the Maures–Tanneron Massif; [58,77,78] for the northern Sardinia; [135] for Corsica. Abbreviations: SA—Sardinia; CO—Corsica; MTM—Maures–Tanneron Massif; ARG—Argenterea Massif; PVX—Pelvoux Massif; BEL—Belledonne Massif; AIG—Aiguilles Rouges Massif.

The available structural data for Asinara Island demonstrate that the Castellaccio and the Punta Sabina intrusive units intruded into the country rocks after the main regional D_2 phase but still suffered minor stress-induced recrystallization. It is not clear the chronology between the emplacement of the two units and the development of the D_3 phase because this phase is not well evident in the field as, in the metamorphic rocks, it is only locally recorded. However, the dynamic recrystallization and deformation of the magmatic bodies were likely triggered by the same shortening that locally developed D_3 structures during the ending of the regional transpressional event when deformation occurred under temperature-decreasing conditions. Unambiguous crosscutting relations, visible in the field, revealed that after the intrusion of the Castellaccio and Punta Sabina units, the emplacement of the sheeted dyke complex started (Figure 2). Dykes intruded progressively into a rock volume that was already deeply affected by the D_2 phase. This is evidenced by the occurrence of many dykes that are sub-parallel to the S_2 foliation (Figures 2 and 3E) or that crosscut the S_2 foliation at a small angle. In some places, dykes intruded into a crust that was also deformed by the D_3, as evidenced by the presence of some dykes that mimic the S_2 foliation deformed by F_3 folds (Figure 3F). Because the progressive nature of the formation of this dyke complex is accompanied by a progressive decrease in deformation until it reaches completion, we observed variability in the range of recorded microstructures in this unit.

In the last years, examples of temporal overlapping between the timing of the emplacement of magmatic bodies and the age of transpressional deformation were found in many sectors of the southern part of the Variscan belt, especially of those belonging to the internal zone of the belt involving the east Variscan shear zone (EVSZ; Figures 9 and 10), where a complex alternation of high-strain and low-stain domains is present [67,130]. Several examples are documented in the external crystalline massifs of the Alps. In the Argentera Massif (Figures 1 and 10), ref. [125] recognized the presence of a mylonitic leucogranite, interpreted as a syn-kinematic intrusion, within the Ferriere Mollieres shear zone, a dextral transpressive shear zone crosscutting the massif that started to become active at 340–330 Ma, with the main mylonitic phase dated at ~320 Ma [131,133]. For this leucogranite, ref. [125] obtained a cooling age of 327 $\pm$ 3 Ma based on Rb/Sr analyses on the whole rock and magmatic muscovite grains, and it was interpreted as a syn-kinematic intrusion (Figure 10). In the Aiguilles Rouge Massif (Figures 1 and 10), the syn-tectonic emplacement of sheet-like peraluminous granites, the Vallorcine granite, the Fully granodiorite, and the Montenverse granite were recognized by refs. [127,136,137]. The Vallorcine granite, emplaced at 306.5 $\pm$ 1.5 Ma [127], is bounded by a dextral transpressional shear zone, the Emosson–Beard shear zone (Figure 10), interpreted as a branch of the EVSZ, that started to become active at ~320 Ma (U-Th-Pb on monazite; [130]). Despite this, similarly to the context described in this work, no evident mesoscale fabric is recognized in the granite, and deformation-induced recrystallization appears only at the microscale [130].

Recently, ref. [124] performed a detailed study of the Camarat granitic complex in the Maures–Tanneron Massif (southern France; Figure 1) and the relative dykes emplaced in the migmatitic internal zone of this massif. According to these Authors, the intrusion was constrained at ~305 Ma (304.5 $\pm$ 3.3 Ma, zircon date; 303.5 $\pm$ 4.0 Ma, monazite date). Magmatic lineation, highlighted by anisotropy of magnetic susceptibility analysis, is oriented coherently with the sub-horizontal mineral lineation observed in the surrounding migmatites, formed during the late-Variscan transpression phase, that started at ~325 Ma in this portion of Variscides (U-Th-Pb on monazite; [129,130]). Therefore, both structural and geochronological arguments suggest a (late-) syn-tectonic emplacement for the dykes. Remaining in the Maures Massif, a large intrusion known as the Plan de la Tour granite is in the internal zone of the belt (Figure 11).

and geochronological arguments suggest a (late-) syn-tectonic emplacement for the dykes. Remaining in the Maures Massif, a large intrusion known as the Plan de la Tour granite is in the internal zone of the belt (Figure 11).

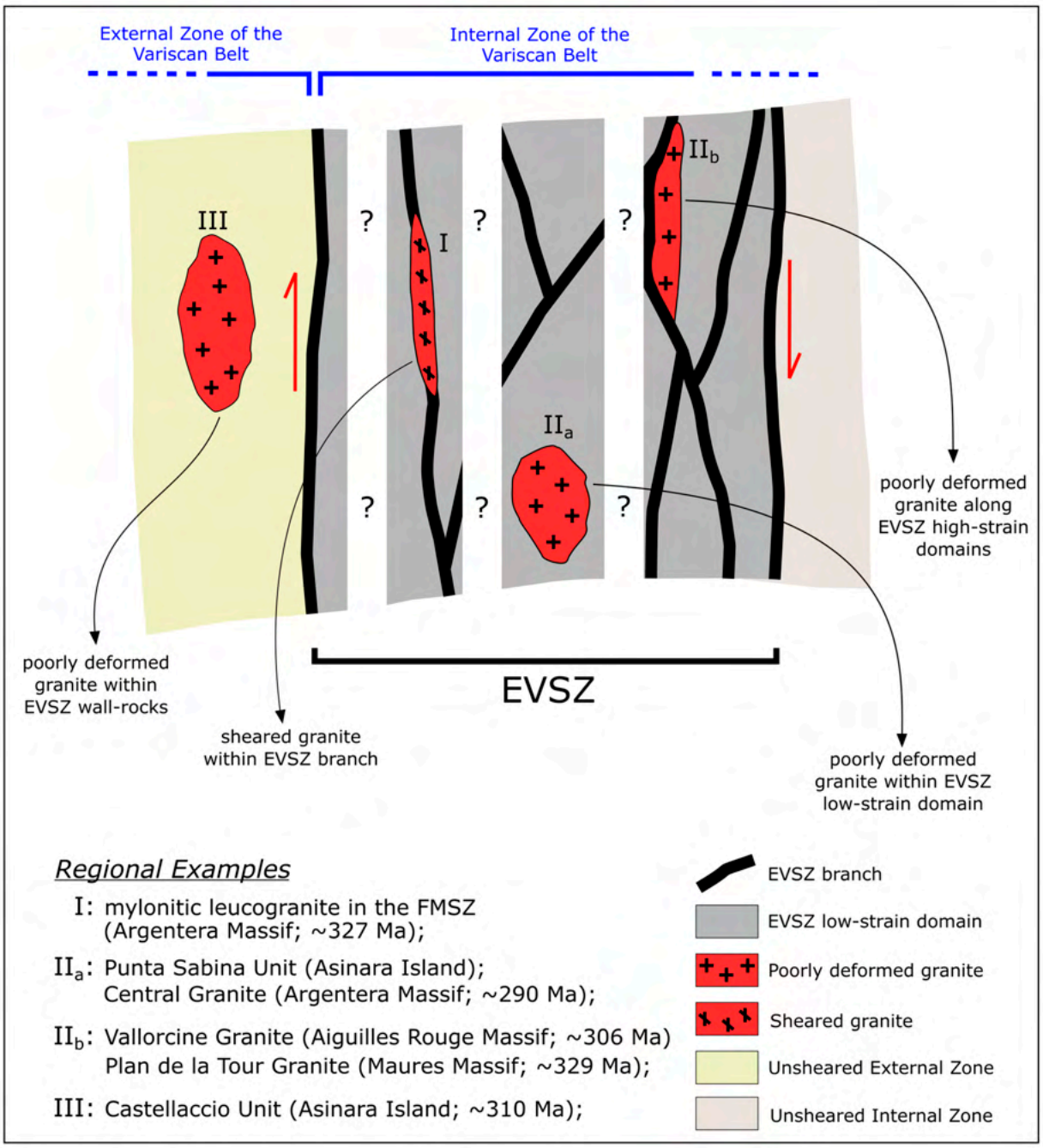

Figure 11. Conceptual sketch (not to scale) summarizing the possible position of the three main groups of intrusions in relation to the internal and external zones of the Variscan belt and of the EVSZ network in plain view.

This intrusion is bounded by the shear zones, the Joyouse Fault and the prosecution of the Grimaud Fault. The evolution of this granite is constrained thanks to U-Th-Pb dating of monazite, its emplacement started at 329 ± 3 Ma [123] and ended at the Carboniferous–Permian transition [138], therefore falling perfectly within the age range of transpressional deformation in this sector of the belt. The intrusion of granites in this sector is coupled with the formation of large-scale antiform structures, that are generally cored by late orogenic granitoids structurally concordant with the surrounding migmatite [139–141]. All these observations are in good agreement with a model of granite emplacement in the context of active deformation at a regional scale.

The emplacement of granitoids in conditions of active late-Variscan deformation is also recognized in other sectors of the Variscan belt. Refs. [47,48], using the same approach

The emplacement of granitoids in conditions of active late-Variscan deformation is also recognized in other sectors of the Variscan belt. Refs. [47,48], using the same approach that we applied in this work, recognized in the Peloritani Mountains and the Serre batholith (southern Italy; Figure 1) the syn-tectonic emplacement of trondhjemite and granites within sheared high-grade paragneiss in late-Variscan time (between 310 and 300 Ma). They interpreted this deformation as linked to the activity of the regional-scale system of interconnected transpressional shear zones of the EVSZ and concluded that their study areas occupied a marginal part of this network even if it is not completely clear if those areas were directly involved in the main shear zone network, and therefore they represent low-strain domains [129], or if they were part of the wall rocks proximal to the network.

Those data demonstrate that granitic intrusions were emplaced in all the sectors of the Mediterranean part of the Variscides accompanying, during the vanishing of the European Variscan orogeny, the exhumation of the ductile lower crust linked to the onset of the transpressional regime characterizing this sector of the belt.

Considering the structural and geochronological data described above, we can recognize three main groups of intrusions at the scale of this sector of the Variscan belt and respect to the EVSZ (Figures 10 and 11). The first group is represented by syn- to late-tectonics granitoids intruded directly along the branches of the EVSZ network (type I in Figure 11) and therefore they are strongly sheared. The second group (type II in Figure 11) comprises magmatic rocks that intruded into the low-strain domains of the EVSZ, poorly affected (type II_a in Figure 11) or marginally affected (type II_b in Figure 11) by shear deformation, within the high-grade internal zone of the belt (Figure 11). The last group of intrusions are hosted in the wall rocks of the EVSZ network (type III in Figure 11). Because of their peculiar position and because they probably are emplaced in the late stage of transpression [125], the last two groups record the deformation only to a minimal extent and, based on field relationships alone, they may appear, at first glance, as post-tectonic intrusions.

In conclusion, the emplacement of widespread late-Variscan granitoids broadly corresponds to the late stages of the crustal-scale transpressional deformation recorded in many sectors of the southern Variscides. This reveals how in the latest phases of the Variscan orogeny, a close relationship between transpressional deformation, exhumation of the deep crust and magmatism occurred. To completely unravel the relationship among all these processes, characterizing the final amalgamation of this sector of Pangea, it is necessary to consider updated, and more complex, tectonic models. Moreover, more detailed analyses, such as those described in this work, conducted with a systematic approach in different places of the Variscan belt are needed. These analyses would allow us to find further differences in the magmatic bodies that could be used as a tool to understand the role of important variables such as (i) the time of emplacement during the Variscan period; (ii) the position of the magmatic bodies concerning the main tectonic structures of the chain; and (iii) the crustal level into which they intrude.

6. Conclusions

The microstructural analysis highlights that the intrusive rocks that crop out in Asinara Island recorded tectonic stress during the cooling of magmatic bodies, even if a prominent mesoscale fabric is absent. The complete sequence of deformation microstructures revealed recrystallization operating from sub-magmatic to low-temperature sub-solidus conditions. Deformation-induced recrystallization supports how magmatic rocks are emplaced under conditions of late and weak but still active, deformation probably linked to the late-Variscan transpression, as suggested by geochronological arguments and regional geological context. The features described in the study area are comparable to those described in other sectors of the Variscan belt in the Mediterranean area, demonstrating that many granitic

intrusions were emplaced during the latest stage of middle/lower crust exhumation linked to active transpression.

Microstructures occurring in such rocks represent a key record of the latest but active (and weak) deformation during the final stage of a regional-scale transpressional regime. A detailed and multidisciplinary study conducted systematically in other late-Variscan intrusive bodies such as those described in this work could refine the proposed tectonic models and shed new light on the complex link between transpressional deformation, exhumation of the deep crust and magmatism that characterizes the final phases of the Variscan orogeny and the amalgamation of the southern European part of Pangea.

Author Contributions: Conceptualization, D.P. and M.S.; methodology, D.P., M.S., S.I., C.M., and R.C.; software, M.S.; validation, D.P., M.S., S.I., C.M., and R.C.; formal analysis, D.P. and M.S.; investigation, D.P. and M.S.; resources, D.P. and M.S.; data curation, D.P. and M.S.; writing—original draft preparation, D.P., M.S., S.I., C.M., and R.C.; writing—review and editing, D.P., M.S., S.I., C.M., and R.C.; funding acquisition, D.P., M.S., S.I., C.M., and R.C. All authors have read and agreed to the published version of the manuscript.

Funding: This research has been supported by the funds of the CARG Project—Geological Map of Italy 1: 50,000. S.I., C.M. and R.C. acknowledge scientific support from Università di Torino funds (ex-60% 2023–2024, resp. C.M., and S.I.).

Data Availability Statement: The original contributions presented in this study are included in the article. Further inquiries can be directed to the corresponding author.

Acknowledgments: We wish to thank Simone Vezzoni for the useful discussions about the features of the various magmatic rocks of the studied area. We thank three anonymous reviewers and the Editor for their comments that improved the manuscript.

Conflicts of Interest: The authors declare no conflicts of interest.

References

1. Paterson, S.R.; Fowler, T.K. Extensional pluton-emplacement models: Do they work for large plutonic complexes? *Geology* **1993**, *21*, 781–784. [CrossRef]
2. Román-Berdiel, T. Geometry of granite emplacement in the upper crust: Contributions of analogue modelling. *Geol. Soc. Spec. Publ.* **1999**, *168*, 77–94. [CrossRef]
3. Corti, G.; Bonini, M.; Conticelli, S.; Innocenti, F.; Manetti, P.; Sokoutis, D. Analogue modelling of continental extension: A review focused on the relations between the patterns of deformation and the presence of magma. *Earth-Sci. Rev.* **2003**, *63*, 169–247. [CrossRef]
4. Dini, A.; Westerman, D.S.; Innocenti, F.; Rocchi, S. Magma emplacement in a transfer zone: The Miocene mafic Orano dyke swarm of Elba Island, Tuscany, Italy. *Geol. Soc. Spec. Publ.* **2008**, *302*, 131–148. [CrossRef]
5. Tack, L.; Wingate, M.T.D.; De Waele, B.; Meert, J.; Belousova, E.; Griffin, B.; Tahon, A.; Fernandez-Alonso, M. The 1375 Ma "Kibaran event" in Central Africa: Prominent emplacement of bimodal magmatism under extensional regime. *Precambrian Res.* **2010**, *180*, 63–84. [CrossRef]
6. Vezzoni, S.; Rocchi, S.; Dini, A. Lateral extrusion of a thermally weakened pluton overburden (Campiglia Marittima, Tuscany). *Int. J. Earth Sci. (Geol. Rundsch.)* **2017**, *107*, 1343–1355. [CrossRef]
7. Brogi, A.; Caggianelli, A.; Liotta, D.; Zucchi, M.; Spina, A.; Capezzuoli, E.; Casini, A.; Buracchi, E. The Gavorrano monzogranite (Northern Apennines): An updated review of host rock protoliths, thermal metamorphism and tectonic setting. *Geosciences* **2021**, *11*, 124. [CrossRef]
8. Collins, W.J.; Sawyer, W. Pervasive granitoid magma transfer through the lower–middle crust during non-coaxial compressional deformation. *J. Metamorph. Geol.* **1996**, *14*, 565–579. [CrossRef]
9. Hutton, D.H.W. Syntectonic Granites and the Principle of Effective Stress: A General Solution to the Space Problem? In *Granite: From Segregation of Melt to Emplacement Fabrics, Petrology and Structural Geology*; Bouchez, J.L., Hutton, D.H.W., Stephens, W.E., Eds.; Springer: Dordrecht, 1997; Volume 8, pp. 189–197. [CrossRef]
10. Kalakay, T.J.; John, B.E.; Lageson, D.R. Fault-controlled pluton emplacement in the Sevier fold-and-thrust belt of southwest Montana, USA. *J. Struct. Geol.* **2001**, *23*, 1151–1165. [CrossRef]
11. Tibaldi, A. Volcanism in compressional tectonic settings: It is possible? *Geophys. Res. Lett.* **2005**, *32*, L06309. [CrossRef]

12. Galland, O.; Cobbold, P.R.; de Bremond d'Ars, J.; Hallot, E. Rise and emplacement of magma during horizontal shortening of the brittle crust: Insights from experimental modelling. *J. Geophys. Res.* **2007**, *112*, B06402. [CrossRef]
13. Galland, O.; Hallot, E.; Cobbold, P.R.; Ruffet, G.; de Bremond d'Ars, J. Volcanism in compressional Andean setting: A structural and geochronological study of Tromen volcano (Nequén province, Argentina). *Tectonics* **2007**, *26*, TC4010. [CrossRef]
14. Mazzarini, F.; Fornaciai, A.; Bistacchi, A.; Pasquarè, F.A. Fissural volcanism, polygenetic volcanic fields, and crustal thickness in the Payen Volcanic Complex on the central Andes foreland (Mendoza, Argentina). *Geochem. Geophys. Geosyst.* **2008**, *9*, Q09002. [CrossRef]
15. D'Lemos, R.S.; Brown, M.; Strachan, R.A. Granite magma generation, ascent and emplacement within a transpressional orogen. *J. Geol. Soc. Lond.* **1992**, *149*, 487–496. [CrossRef]
16. Hutton, D.H.W.; Reavy, R.S. Strike-slip tectonics and granite petrogenesis. *Tectonics* **1992**, *11*, 960–967. [CrossRef]
17. Brown, M. The generation, segregation, ascent and emplacement of granite magma. *Earth-Sci. Rev.* **1994**, *36*, 83–130. [CrossRef]
18. Vigneresse, J.L. Control of granite emplacement by regional deformation. *Tectonophysics* **1995**, *249*, 173–186. [CrossRef]
19. Román-Berdiel, T.; Gapais, D.; Brun, J.P. Granite intrusion along strike-slip zones in experiment and nature. *Am. J. Sci.* **1997**, *297*, 651–678. [CrossRef]
20. Salvini, F.; Brancolini, G.; Busetti, M.; Storti, F.; Mazzarini, F.; Coren, F. Cenozoic geodynamics of the Ross Sea region, Antarctica: Crustal extension, intraplate strike-slip faulting, and tectonic inheritance. *J. Geophys. Res.* **1997**, *102*, 24669–24696. [CrossRef]
21. Rosenberg, C.L. Shear zones and magma ascent: A model based on a review of the Tertiary magmatism in the Alps. *Tectonics* **2004**, *23*, TC2003. [CrossRef]
22. Liotta, D.; Festa, V.; Caggianelli, A.; Prosser, G.; Pascazio, A. Mid-crustal shear zone evolution in a syn-tectonic late Hercynian granitoid (Sila Massif, Calabria, southern Italy). *Int. J. Earth. Sci. (Geol. Rundsch.)* **2004**, *93*, 400–413. [CrossRef]
23. Corti, G.; Moratti, G.; Sani, F. Relations between surface faulting and granite intrusions in analogue models of strike-slip deformation. *J. Struct. Geol.* **2005**, *27*, 1547–1562. [CrossRef]
24. Boutonnet, E.; Leloup, P.H.; Arnaud, N.; Paquette, J.-L.; Davis, W.J.; Hattori, K. Synkinematic magmatism, heterogeneous deformation, and progressive strain localization in a strike-slip shear zone: The case of the right-lateral Karakorum fault. *Tectonics* **2012**, *31*, TC4012. [CrossRef]
25. Vezzoni, S.; Biagioni, C.; D'Orazio, M.; Pieruccioni, D.; Galanti, Y.; Petrelli, M.; Molli, G. Evidence of Permian magmatism in the Alpi Apuane metamorphic complex (Northern Apennines, Italy): New hints for the geological evolution of the basement of the Adria plate. *Lithos* **2018**, *318–319*, 104–123. [CrossRef]
26. Vieira, D.T.; Koester, E.; Ramos, R.C.; Porcher, C.C.; D'Ávila Fernandes, L.A. SHRIMP U-Pb zircon ages for the synkinematic magmatism in the Dorsal de Canguçu Transcurrent Shear Zone, Dom Feliciano Belt (Brazil): Tectonic implications. *J. South Am. Earth Sci.* **2020**, *100*, 102603. [CrossRef]
27. Román-Berdiel, T.; Gapais, D.; Burg, J.P. Analogue models of laccolith formation. *J. Struct. Geol.* **1995**, *17*, 1337–1346. [CrossRef]
28. Petford, N.; Cruden, A.R.; McCaffrey, K.J.W.; Vigneresse, J.L. Granite magma formation, transport and emplacement in the Earth's crust. *Nature* **2000**, *408*, 669–673. [CrossRef]
29. Kavanagh, J.L.; Menand, T.; Sparks, R.S.J. An experimental investigation of sill formation and propagation in layered elastic media. *Earth Planet. Sci. Lett.* **2006**, *245*, 799–813. [CrossRef]
30. Mazzarini, F.; Musumeci, G.; Montanari, D.; Corti, G. Relations between deformation and upper crustal magma emplacement in laboratory physical models. *Tectonophysics* **2010**, *484*, 139–146. [CrossRef]
31. Beaumont, C.; Jamieson, R.; Nguyen, M. Models of large, hot orogens containing a collage of reworked and accreted terranes. *Can. J. Earth Sci.* **2010**, *47*, 485–515. [CrossRef]
32. Butler, R.W.H.; Harris, N.B.W.; Whittington, A.G. Interactions between deformation, magmatism and hydrothermal activity during active crustal thickening: A field example from Nanga Parbat, Pakistan Himalayas. *Mineral. Mag.* **1997**, *61*, 37–52. [CrossRef]
33. Paterson, S.R.; Tobisch, O.T. Using pluton ages to date regional deformations: Problems with commonly used criteria. *Geology* **1988**, *16*, 1108–1111. [CrossRef]
34. Evans, N.G.; Gleizes, G.; Leblanc, D.; Bouchez, J.L. Syntectonic emplacement of the Maladeta granite (Pyrenees) deduced from relationships between Hercynian deformation and contact metamorphism. *J. Geol. Soc. Lond.* **1998**, *155*, 209–216. [CrossRef]
35. Vezzoni, S.; Pieruccioni, D.; Galanti, Y.; Biagioni, C.; Dini, A. Permian hydrothermal alteration preserved in polymetamorphic basement and constraints for ore-genesis (Alpi Apuane, Italy). *Geosciences* **2020**, *10*, 399. [CrossRef]
36. Casini, L.; Maino, M.; Langone, A.; Oggiano, G.; Corvò, S.; Estrada, J.R.; Liesa, M. HTLP metamorphism and fluid-fluxed melting during multistage anatexis of continental crust (N Sardinia, Italy). *J. Metamorph. Geol.* **2023**, *41*, 25–57. [CrossRef]
37. Gleizes, G.; Leblanc, D.; Olivier, P.; Bouchez, J. Strain partitioning in a pluton during emplacement in transpressional regime: The example of the Néouvielle granite (Pyrenees). *Int. J. Earth Sci.* **2001**, *90*, 325–340. [CrossRef]
38. Pawley, M.J.; Collins, W.J. The development of contrasting structures during the cooling and crystallisation of a syn-kinematic pluton. *J. Struct. Geol.* **2002**, *24*, 469–483. [CrossRef]

39. Gloaguen, E.; Branquet, Y.; Chauvet, A.; Bouchot, B.; Barbanson, L.; Vigneresse, J.-L. Tracing the magmatic/hydrothermal transition in regional low-strain zones: The role of magma dynamics in strain localization at pluton roof, implications for intrusion-related gold deposits. *J. Struct. Geol.* **2014**, *58*, 108–121. [CrossRef]
40. Ludovic, A.M.; Maurice, K.; Martial, F.E.; Jules, T.K.; Julios, E.A.; Cliff, C.K.S.; Belmien, S.Y.R.; Blandine, K.T.A.; Lauraine, A.F. Field observations and microstructural evidence of syntectonic emplacement of the Ngwi granitic plutons (central Cameroon domain). *Arab. J. Geosci.* **2021**, *14*, 1497. [CrossRef]
41. de Luchi, M.G.L.; Rapalini, A.E.; Tomezzoli, R.N. Magnetic fabric and microstructures of Late Paleozoic granitoids from the North Patagonian Massif: Evidence of a collision between Patagonia and Gondwana? *Tectonophysics* **2010**, *494*, 118–137. [CrossRef]
42. Bouchez, J.L.; Gleizes, G.; Djouadi, T.; Rochette, P. Microstructure and magnetic susceptibility applied to emplacement kinematics of granites: The example of the Foix pluton (French Pyrenees). *Tectonophysics* **1990**, *184*, 157–171. [CrossRef]
43. Vernon, R.H.; Johnson, S.E.; Melis, E.A. Emplacement-related microstructures in the margin of a deformed pluton: The San José tonalite, Baja California, México. *J. Struct. Geol.* **2004**, *26*, 1867–1884. [CrossRef]
44. Casini, L.; Cuccuru, S.; Maino, M.; Oggiano, G.; Tiepolo, M. Emplacement of the Arzachena Pluton (Corsica–Sardinia Batholith) and the geodynamics of incoming Pangaea. *Tectonophysics* **2012**, *544–545*, 31–49. [CrossRef]
45. Secchi, F.; Casini, L.; Cifelli, F.; Naitza, S.; Carta, E.; Oggiano, G. Syntectonic magmatism and reactivation of collisional structures during late-Variscan shearing (SW Sardinia, Italy). *Int. J. Earth Sci. (Geol. Rundsch.)* **2022**, *111*, 1469–1490. [CrossRef]
46. Castro, A. On granitoid emplacement and related structures. A review. *Geol. Rundsch.* **1987**, *76*, 101–124. [CrossRef]
47. Fazio, E.; Fiannacca, P.; Russo, D.; Cirrincione, R. Submagmatic to solid-state deformation microstructures recorded in cooling granitoids during exhumation of Late-Variscan crust in North-Eastern Sicily. *Geosciences* **2020**, *10*, 311. [CrossRef]
48. Fiannacca, P.; Russo, D.; Fazio, E.; Cirrincione, R.; Mamtani, M.A. Fabric analysis in upper crustal post-collisional granitoids from the Serre Batholith (Southern Italy): Results from microstructural and AMS investigations. *Geosciences* **2021**, *11*, 414. [CrossRef]
49. Cappelli, B.; Carmignani, L.; Castorina, F.; Di Pisa, A.; Oggiano, G.; Petrini, R. A Hercynian suture zone in Sardinia: Geological and geochemical evidence. *Geodin. Acta* **1992**, *5*, 101–118. [CrossRef]
50. Carmignani, L.; Carosi, R.; Di Pisa, A.; Gattiglio, M.; Musumeci, G.; Oggiano, G.; Pertusati, P.C. The Hercynian chain in Sardinia (Italy). *Geodin. Acta* **1994**, *7*, 31–47. [CrossRef]
51. Carosi, R.; Palmeri, R. Orogen-parallel tectonic transport in the Variscan belt of northeastern Sardinia (Italy): Implications for the exhumation of medium-pressure metamorphic rocks. *Geol. Mag.* **2002**, *139*, 497–511. [CrossRef]
52. Franke, W. Tectonostratigraphic units in the Variscan belt of central Europe. *Geol. Soc. Am. Spec. Pap.* **1989**, 67–90. [CrossRef]
53. Matte, P. The Variscan collage and orogeny (480–290 Ma) and the tectonic definition of the Armorica microplate: A review. *Terra Nova* **2001**, *13*, 122–128. [CrossRef]
54. Stampfli, G.M.; Hochard, C.; Vérard, C.; Wilhem, C.; von Raumer, J. The formation of Pangea. *Tectonophysics* **2013**, *593*, 1–19. [CrossRef]
55. Domeier, M.; Torsvik, T.H. Plate tectonics in the late Paleozoic. *Geosci. Front.* **2014**, *5*, 303–350. [CrossRef]
56. von Raumer, J.F.; Busy, F.; Schaltegger, U.; Schulz, B.; Stampfli, G.M. Pre-Mesozoic Alpine basements—Their place in the European Paleozoic framework. *Geol. Soc. Am. Bull.* **2013**, *125*, 89–108. [CrossRef]
57. Carosi, R.; Frassi, C.; Montomoli, C. Deformation during exhumation of medium- and high-grade metamorphic rocks in the Variscan chain in northern Sardinia (Italy). *Geol. J.* **2009**, *44*, 280–305. [CrossRef]
58. Carosi, R.; Petroccia, A.; Iaccarino, S.; Simonetti, M.; Langone, A.; Montomoli, C. Kinematics and timing constraints in a transpressive tectonic regime: The example of the Posada-Asinara Shear Zone (NE Sardinia, Italy). *Geosciences* **2020**, *10*, 288. [CrossRef]
59. Cruciani, G.; Montomoli, C.; Carosi, R.; Franceschelli, M.; Puxeddu, M. Continental collision from two perspectives: A review of Variscan metamorphism and deformation in northern Sardinia. *Per. Min.* **2015**, *84*, 657–699. [CrossRef]
60. Cocco, F.; Funedda, A. Mechanical influence of inherited folds in thrust development: A case study from the Variscan fold-and-thrust belt in SW Sardinia (Italy). *Geosciences* **2021**, *11*, 276. [CrossRef]
61. Casini, L.; Funedda, A.; Oggiano, G. A balanced foreland–hinterland deformation model for the Southern Variscan belt of Sardinia, Italy. *Geol. J.* **2010**, *45*, 634–649. [CrossRef]
62. Cocco, F.; Oggiano, G.; Funedda, A.; Loi, A.; Casini, L. Stratigraphic, magmatic and structural features of Ordovician tectonics in Sardinia (Italy): A review. *J. Iber. Geol.* **2018**, *44*, 619–639. [CrossRef]
63. Petroccia, A.; Forshaw, J.B.; Lanari, P.; Iaccarino, S.; Montomoli, C.; Carosi, R. Pressure and temperature estimation in greenschist-facies metapelites: An example from the Variscan Belt in Sardinia. *J. Metamorph. Geol.* **2025**, *43*, 21–46. [CrossRef]
64. Giacomini, F.; Bomparola, R.M.; Ghezzo, C.; Guldbransen, H. The geodynamic evolution of the Southern European Variscides: Constraints from the U/Pb geochronology and geochemistry of the lower Palaeozoic magmatic-sedimentary sequences of Sardinia (Italy). *Contrib. Mineral. Petrol.* **2006**, *152*, 19–42. [CrossRef]
65. Elter, F.M.; Musumeci, G.; Pertusati, P.C. Late Hercynian shear zones in Sardinia. *Tectonophysics* **1990**, *176*, 387–404. [CrossRef]

66. Iacopini, D.; Carosi, R.; Montomoli, C.; Passchier, C.W. Strain analysis and vorticity of flow in the Northern Sardinian Variscan Belt: Recognition of a partitioned oblique deformation event. *Tectonophysics* **2008**, *446*, 77–96. [CrossRef]
67. Carosi, R.; Montomoli, C.; Iaccarino, S.; Benetti, B.; Petroccia, A.; Simonetti, M. Constraining the timing of evolution of shear zones in two collisional orogens: Fusing structural geology and geochronology. *Geosciences* **2022**, *12*, 231. [CrossRef]
68. Carosi, R.; Di Pisa, A.; Iacopini, D.; Montomoli, C.; Oggiano, G. The structural evolution of the Asinara Island (NW Sardinia, Italy). *Geodin. Acta* **2004**, *17*, 309–329. [CrossRef]
69. Franceschelli, M.; Puxeddu, M.; Cruciani, G. Variscan metamorphism in Sardinia, Italy: Review and discussion. *J. Virtual Explor.* **2005**, *19*, 2. [CrossRef]
70. Franceschelli, M.; Memmi, I.; Pannuti, F.; Ricci, C.A. Diachronous metamorphic equilibria in the Hercynian basement of northern Sardinia, Italy. *Geol. Soc. Spec. Publ.* **1989**, *43*, 371–375. [CrossRef]
71. Di Pisa, A.; Oggiano, G.; Talarico, F. Post collisional tectono-metamorphic evolution in the axial zone of the Hercynian belt in Sardinia: The example from the Asinara island. *Doc. B.R.G.M.* **1993**, *219*, 216–217.
72. Strada, E.; Talarico, F.M.; Florindo, F. Magnetic petrology of variably retrogressed eclogites and amphibolites: A case study from the Hercynian basement of northern Sardinia (Italy). *J. Geophys. Res.* **2006**, *111*, B12S26. [CrossRef]
73. Carosi, R.; Montomoli, C.M.; Iacopini, D.; Petroccia, A.; Simonetti, M.; Oggiano, G. Geology of the Asinara Island (Sardinia, Italy). *J. Maps* **2024**, *20*, 2317136. [CrossRef]
74. Simonetti, M.; Pieruccioni, D.; Carosi, R.; Montomoli, C.; Iaccarino, S.; Zucchi, M. A review of criteria, methods, and standards for mapping crystalline terrains: Integrating field geology and analytical data. *Ital. J. Geosci.* **2024**, *143*, 426–454. [CrossRef]
75. Cruciani, G.; Franceschelli, M.; Massonne, H.J.; Carosi, R.; Montomoli, C. Pressure–temperature and deformational evolution of high-pressure metapelites from Variscan NE Sardinia, Italy. *Lithos* **2013**, *175–176*, 272–284. [CrossRef]
76. Cruciani, G.; Franceschelli, M.; Carosi, R.; Montomoli, C. P-T path from garnet zoning in pelitic schist from NE Sardinia, Italy: Further constraints on the metamorphic and tectonic evolution of the north Sardinia Variscan belt. *Lithos* **2022**, *428–429*, 106836. [CrossRef]
77. Di Vincenzo, G.; Carosi, R.; Palmeri, R. The relationship between tectono-metamorphic evolution and Argon isotope records in white mica: Constraints from in situ ^{40}Ar-^{39}Ar laser analysis of the Variscan Basement of Sardinia. *J. Petrol.* **2004**, *45*, 1013–1043. [CrossRef]
78. Carosi, R.; Montomoli, C.; Tiepolo, M.; Frassi, C. Geochronological constraints on post-collisional shear zones in the Variscides of Sardinia (Italy): Post-collisional shear zones in the Variscides of Sardinia. *Terra Nova* **2012**, *24*, 42–51. [CrossRef]
79. Franceschelli, M.; Puxeddu, M.; Cruciani, G.; Utzeri, D. Metabasites with eclogite facies relics from Variscides in Sardinia, Italy: A review. *Int. J. Earth Sci.* **2007**, *96*, 795–815. [CrossRef]
80. Cocco, F.; Attardi, A.; Deidda, M.L.; Fancello, D.; Funedda, A.; Naitza, S. Passive structural control on skarn mineralization localization: A case study from the Variscan Rosas Shear Zone (SW Sardinia, Italy). *Minerals* **2022**, *12*, 272. [CrossRef]
81. Ghezzo, C.; Orsini, J.B. Lineamenti strutturali e composizionali del batolite ercinico Sardo-Corso in Sardegna. *Guid. Alla Geol. Del Paleozoico Sardo* **1982**, 165–182.
82. Rossi, P.; Cocherie, A. Genesis of a Variscan batholith: Field, mineralogical and geochemical evidence from the Corsica-Sardinia batholith. *Tectonophysics* **1991**, *195*, 319–346. [CrossRef]
83. Cocherie, A.; Rossi, P.; Fanning, C.M.; Guerrot, C. Comparative use of TIMS and SHRIMP for U–Pb zircon dating of A-type granites and mafic tholeiitic layered complexes and dykes from the Corsican Batholith (France). *Lithos* **2005**, *82*, 185–219. [CrossRef]
84. Casini, L.; Cuccuru, S.; Puccini, A.; Oggiano, G.; Rossi, P. Evolution of the Corsica–Sardinia Batholith and late-orogenic shearing of the Variscides. *Tectonophysics* **2015**, *646*, 65–78. [CrossRef]
85. Ferré, E.C.; Leake, B.E. Geodynamic significance of early orogenic high-K crustal and mantle melts: Example of the Corsica Batholith. *Lithos* **2001**, *59*, 47–67. [CrossRef]
86. Paquette, J.L.; Ménot, R.P.; Pin, C.; Orsini, J.B. Episodic short-lived granitic pulses in a post-collisional setting: Evidence from precise U–Pb zircon dating through a crustal cross-section in Corsica. *Chem. Geol.* **2003**, *198*, 1–20. [CrossRef]
87. Rossi, P.; Chavez, J.Y.; Cocherie, A. Age varisque précoce du plutonisme magnésio-potassique en Corse occidentale: Conséquences géodynamiques. *C. R. Acad. Sci.* **1988**, *307*, 1541–1547.
88. Laporte, D.; Fernandez, A.; Orsini, J.B. Le complexe d'Ile Rousse, Balagne, Corse du Nord-Ouest: Pétrologie et cadre de mise en place des granitoides magnésiopotassiques. *Géol. Fr.* **1991**, *4*, 15–30.
89. Gaggero, L.; Oggiano, G.; Buzzi, L.; Slejko, F.F.; Cortesogno, L. Post-variscan mafic dikes from the late orogenic collapse to the Tethyan rift: Evidence from Sardinia. *Ofioliti* **2007**, *32*, 15–37.
90. Oggiano, G.; Casini, L.; Mameli, P.; Rossi, P. Long-lived dextral strike-slip tectonics in the southern Variscan Belt: Evidence from two syn-kinematic intrusions in north Sardinia. *Géol. Fr.* **2007**, *2*, 142.
91. Piazolo, S.; Passchier, C.W. Experimental modeling of viscous inclusions in a circular high-strain shear rig: Implications for the interpretation of shape fabrics and deformed enclaves. *J. Geophys. Res.* **2002**, *107*, ETG 11-1–ETG 11-15. [CrossRef]

92. Stipp, M.; Stunitz, H.; Heilbronner, R.; Schmid, S.M. The eastern Tonale fault zone: A "natural laboratory" for crystal plastic deformation of quartz over a temperature range from 250 to 700 °C. *J. Struct. Geol.* **2002**, *24*, 1864–1884. [CrossRef]
93. Passchier, C.W.; Trouw, R.A.J. *Microtectonics*, 2nd ed.; Springer: Berlin, 2005; ISBN 978-3-540-64003-5. [CrossRef]
94. Law, R.D. Deformation thermometry based on quartz c-axis fabrics and recrystallization microstructures: A review. *J. Struct. Geol.* **2014**, *66*, 129–161. [CrossRef]
95. Cuccuru, S.; Casini, L.; Oggiano, G.; Simula, E.N. Structure of the Castellaccio Pluton (Asinara Island, Italy). *J. Maps* **2018**, *14*, 293–302. [CrossRef]
96. Langone, A.; Corvò, S.; Maino, M.; Casini, L. Incremental growth of a shallow S-type megacrystic pluton (Asinara Isl., NW Sardinia, Italy). *Abstr. Book SGI-SIMP* **2022**, 1023. Available online: https://www.socgeol.it/ (accessed on 11 March 2025).
97. Blumenfeld, P.; Mainprice, D.; Bouchez, J.L. C-slip in quartz from subsolidus deformed granite. *Tectonophysics* **1986**, *127*, 97–115. [CrossRef]
98. Mainprice, D.; Bouchez, J.L.; Blumenfeld, P.; Tubià, J.M. Dominant c-slip in naturally deformed quartz: Implications for dramatic plastic softening at high temperature. *Geology* **1986**, *14*, 819–822. [CrossRef]
99. Kruhl, J.H. Prism- and basal-plane parallel subgrain boundaries in quartz: A microstructural geothermobarometer. *J. Metamorph. Geol.* **1996**, *14*, 581–589. [CrossRef]
100. Vidal, J.L.; Kubin, L.; Debat, P.; Soula, J.L. Deformation and dynamic recrystallisation of K-feldspar augen in orthogneiss from Montagne Noir, Occitania. *Lithos* **1980**, *13*, 247–255. [CrossRef]
101. Olsen, T.S.; Kohlstedt, D.L. Natural deformation and recrystallization of some intermediate plagioclase feldspars. *Tectonophysics* **1985**, *111*, 107–131. [CrossRef]
102. Pryer, L.L. Microstructures in feldspars from a major crustal thrust zone: The Grenville Front, Ontario, Canada. *J. Struct. Geol.* **1993**, *15*, 21–36. [CrossRef]
103. Kruse, R.; Stünitz, H. Deformation mechanisms and phase distribution in mafic high-temperature mylonites from the Jotun Nappe, Southern Norway. *Tectonophysics* **1999**, *303*, 223–249. [CrossRef]
104. Altenberger, U.; Wilhelm, S. Ductile deformation of K-feldspar in dry eclogite facies shear zones in the Bergen Arcs, Norway. *Tectonophysics* **2000**, *320*, 107–121. [CrossRef]
105. Simpson, C.; Wintsch, R.P. Evidence for deformation-induced K-feldspar replacement by myrmekite. *J. Metamorph. Geol.* **1989**, *7*, 261–275. [CrossRef]
106. Borges, F.S.; White, S.H. Microstructural and chemical studies of sheared anorthosites, Roneval, South Harris. *J. Struct. Geol.* **1980**, *2*, 273–280. [CrossRef]
107. Tullis, J.; Yund, R.A. Diffusion creep in feldspar aggregates: Experimental evidence. *J. Struct. Geol.* **1991**, *13*, 987–1000. [CrossRef]
108. Warr, L.N. IMA-CNMNC approved mineral symbols. *Mineral. Mag.* **2021**, *85*, 291–320. [CrossRef]
109. Lloyd, G.E.; Freeman, B. Dynamic recrystallization of quartz under greenschist conditions. *J. Struct. Geol.* **1994**, *16*, 867–881. [CrossRef]
110. Ji, S. Deformation microstructure of natural plagioclase. In *Fault Related Rocks—A Photographic Atlas*; Snoke, A., Tullis, J., Todd, V.R., Eds.; Princeton University Press: Princeton, NJ, USA, 1998; pp. 276–277.
111. Ji, S. Kink bands and recrystallization in plagioclase. In *Fault Related Rocks—A Photographic Atlas*; Snoke, A., Tullis, J., Todd, V.R., Eds.; Princeton University Press: Princeton, NJ, USA, 1998; pp. 278–279.
112. Debat, P.; Soula, J.C.; Kubin, L.; Vidal, J.L. Optical studies of natural deformation microstructures in feldspars (gneiss and pegmatites from Occitania, Southern France. *Lithos* **1978**, *11*, 133–145. [CrossRef]
113. Pryer, L.L.; Robin, P.Y.F. Retrograde metamorphic reactions in deforming granites and the origin of flame perthite. *J. Metamorph. Geol.* **1995**, *133*, 645–658. [CrossRef]
114. Christie, J.M.; Raleigh, C.B. The origin of deformation lamellae in quartz. *Am. J. Sci.* **1959**, *257*, 385–407. [CrossRef]
115. Ave L'Allement, H.G.; Carter, N.L. Pressure dependence of quartz deformation lamellae orientations. *Am. J. Sci.* **1971**, *270*, 218–235. [CrossRef]
116. Drury, M.R. Deformation lamellae in metals and minerals. In *Defects and Processes in the Solid State: Geoscience Applications—The McLaren Volume*; Boland, J.N., Fitz Gerald, J.D., Eds.; Elsevier Science Publishers BV: Amsterdam, The Netherlands, 1993; pp. 195–212.
117. Trepmann, C.A.; Stöckhert, B. Quartz microstructures developed during non-steady state plastic flow at rapidly decaying stress and strain rate. *J. Struct. Geol.* **2003**, *25*, 2035–2051. [CrossRef]
118. Wilson, C.J.L. Shear zones in a pegmatite: A study of albite-mica-quartz deformation. *J. Struct. Geol.* **1980**, *2*, 203–209. [CrossRef]
119. Bell, I.A.; Wilson, C.J.L.; McLaren, A.C.; Etheridge, M.A. Kinks in mica: Role of dislocations and (001) cleavage. *Tectonophysics* **1986**, *127*, 49–65. [CrossRef]
120. Stesky, R.M. Mechanisms of high temperature frictional sliding in Westerly granite. *Can. J. Earth Sci.* **1978**, *15*, 361–375. [CrossRef]
121. Kanaori, Y.; Kawakami, S.; Yairi, K. Microstructure of deformed biotite defining foliation in cataclasite zones in granite, central Japan. *J. Struct. Geol.* **1991**, *13*, 777–785. [CrossRef]

122. Bouchez, J.L.; Delas, C.; Gleizes, G.; Nédélec, A.; Cuney, M. Submagmatic microfractures in granites. *Geology* **1992**, *20*, 35–38. [CrossRef]
123. Oliot, E.; Melleton, J.; Schneider, J.; Corsini, M.; Gardien, V.; Rolland, Y. Variscan crustal thickening in the Maures-Tanneron massif (South Variscan belt, France): New in situ monazite U-Th-Pb chemical dating of high-grade rocks. *Bull. Soc. Géol. Fr.* **2015**, *186*, 145–169. [CrossRef]
124. Bolle, O.; Corsini, M.; Diot, H.; Laurent, O.; Melis, R. Late-orogenic evolution of the Southern European Variscan Belt constrained by fabric analysis and dating of the Camarat Granitic Complex and coeval felsic dykes (Maures–Tanneron Massif, SE France). *Tectonics* **2023**, *42*, e2022TC007310. [CrossRef]
125. Musumeci, G.; Colombo, F. Late Visean mylonitic granitoids in the Argentera Massif (western Alps, Italy): Age and kinematic constraints on the Ferrière–Mollières shear zone. *C. R. Geosci.* **2002**, *334*, 213–220. [CrossRef]
126. Ferrara, G.; Malaroda, R. Radiometric age of granitic rocks from the Argentera Massif (Maritime Alps). *Boll. Soc. Geol. It.* **1969**, *88*, 311–320.
127. Bussy, F.; Hernandez, J.; Von Raumer, J. Bimodal magmatism as a consequence of the post-collisional readjustment of the thickened Variscan continental lithosphere (Aiguilles Rouges-Mont Blanc Massifs, Western Alps). *Earth Environ. Sci. Trans. R. Soc. Edinb.* **2000**, 221–233. [CrossRef]
128. Corsini, M.; Rolland, Y. Late evolution of the southern European Variscan belt: Exhumation of the lower crust in a context of oblique convergence. *C. R. Geosci.* **2009**, *341*, 214–223. [CrossRef]
129. Simonetti, M.; Carosi, R.; Montomoli, C.; Corsini, M.; Petroccia, A.; Cottle, J.M.; Iaccarino, S. Timing and kinematics of flow in a transpressive dextral shear zone, Maures Massif (Southern France). *Int. J. Earth Sci. (Geol. Rundsch.)* **2020**, *109*, 2261–2285. [CrossRef]
130. Simonetti, M.; Carosi, R.; Montomoli, C.; Cottle, J.M.; Law, R.D. Transpressive deformation in the Southern European Variscan Belt: New insights from the Aiguilles Rouges Massif (Western Alps). *Tectonics* **2020**, *39*, e2020TC006153. [CrossRef]
131. Simonetti, M.; Carosi, R.; Montomoli, C.; Langone, A.; D'Addario, E.; Mammoliti, E. Kinematic and geochronological constraints on shear deformation in the Ferriere-Mollières shear zone (Argentera-Mercantour Massif, Western Alps): Implications for the evolution of the Southern European Variscan Belt. *Int. J. Earth Sci. (Geol. Rundsch.)* **2018**, *107*, 2163–2189. [CrossRef]
132. Guillot, S.; Ménot, R.-P. Paleozoic evolution of the External Crystalline Massifs of the Western Alps. *Compt. Rend. Geosci.* **2009**, *341*, 253–265. [CrossRef]
133. Simonetti, M.; Carosi, R.; Montomoli, C.; Law, R.D.; Cottle, J.M. Unravelling the development of regional-scale shear zones by a multidisciplinary approach: The case study of the Ferriere-Mollières Shear Zone (Argentera Massif, Western Alps). *J. Struct. Geol.* **2021**, *149*, 104399. [CrossRef]
134. Fréville, K.; Trap, P.; Vanardois, J.; Melleton, J.; Faure, M.; Bruguier, O.; Poujol, M.; Lach, P. Carboniferous tectono-metamorphic evolution of the Variscan crust in the Belledonne-Pelvoux area. *BSGF—Earth Sci. Bull.* **2022**, *193*, 13. [CrossRef]
135. Giacomini, F.; Dallai, L.; Carminati, E.; Tiepolo, M.; Ghezzo, C. Exhumation of a Variscan orogenic complex: Insights into the composite granulitic–amphibolitic metamorphic basement of south-east Corsica (France). *J. Metamorph. Geol.* **2008**, *26*, 403–436. [CrossRef]
136. Genier, F.; Bussy, F.; Epard, J.L.; Baumgartner, L. Water-assisted migmatization of metagraywackes in a Variscan shear zone, Aiguilles-Rouges massif, western Alps. *Lithos* **2008**, *102*, 575–597. [CrossRef]
137. Von Raumer, J.; Bussy, F. Mont Blanc and Aiguilles Rouges geology of their polymetamorphic basement (external massifs, Westerns Alps, France-Switzerland). *Mém. Géol.* **2004**, *42*, 1–210.
138. Gerbault, M.; Schneider, J.; Reverso-Peila, A.; Corsini, M. Crustal exhumation during ongoing compression in the Variscan Maures-Tanneron Massif, France–Geological and thermo-mechanical aspects. *Tectonophysics* **2018**, *746*, 439–458. [CrossRef]
139. Rolland, Y.; Corsini, M.; Demoux, A. Metamorphic and structural evolution of the Maures-Tanneron massif (SE Variscan chain): Evidence of doming along a transpressional margin. *Bull. Soc. Géol. Fr.* **2009**, *180*, 217–230. [CrossRef]
140. Corsini, M.; Bosse, V.; Féraud, G.; Demoux, A.; Crevola, G. Exhumation processes during post-collisional stage in the Variscan belt revealed by detailed $^{40}Ar/^{39}Ar$ study (Tanneron Massif, SE France). *Int. J. Earth Sci.* **2010**, *99*, 327–341. [CrossRef]
141. Schneider, J.; Corsini, M.; Reverso-Peila, A.; Lardeaux, J.M. Thermal and mechanical evolution of an orogenic wedge during Variscan collision: An example in the Maures–Tanneron Massif (SE France). *Geol. Soc. Spec. Publ.* **2014**, *405*, 313–331. [CrossRef]